TECHNISCHE
UNIVERSITÄT
WIEN

DIPLOMARBEIT

Nano-alloy-cluster Katalysatoren für die Wasserstoffproduktion

ausgeführt am

Institut für Materialchemie
der Technischen Universität Wien

unter der Anleitung von

Assoc.Univ.Prof. Dr.in. Noelia Barrabés
Privatdoz. Mag.rer.nat. Dr.rer.nat. Christoph Rameshan

durch

Nicole Müller, BSc.

Wien, im April 2023

MASTER THESIS

Nanoalloy cluster catalysts for hydrogen production

carried out at the

Institute of Materials Chemistry

of TU Wien

under the supervision of

Assoc.Univ.Prof. Dr.in. Noelia Barrabés

Privatdoz. Mag.rer.nat. Dr.rer.nat. Christoph Rameshan

by

Nicole Müller, BSc.

Vienna, in April 2023

Eidesstattliche Erklärung

Ich erkläre hiermit an Eides statt, dass ich die vorliegende Diplomarbeit selbstständig und ohne fremde Hilfe verfasst, andere als die angegebenen Quellen und Hilfsmittel nicht benutzt und die den benutzten Quellen wörtlich und inhaltlich entnommenen Stellen als solche erkenntlich gemacht habe.

Statutory Declaration

I declare that I have authored this thesis independently, that I have not used other than the declared sources / resources, and that I have explicitly marked all material which has been quoted either literally or by content from the used sources.

Zusammenfassung

Seitdem H_2 als vielversprechende Brennstoffquelle interessant geworden ist, haben sich einige Forschungsarbeiten darauf fokussiert, einen effizienten Weg zur Herstellung von H_2 über die Wassergas-Shift-Reaktion (WGSR) durch das effiziente Design von geeigneten Katalysatoren zu finden. Um die Herstellung von effektiven Katalysatoren zu ermöglichen, wird viel Arbeit und Forschung für das Katalystordesign gesteckt. Ein Verständnis der Katalysatorstruktur auf atomarer Ebene sowie, der während der Reaktion ablaufenden Prozesse, ist erforderlich. Ziel dieser Arbeit war es daher, verschiedene Katalysatoren für die WGSR zu entwerfen und mit verschiedenen Analysemethoden zu testen, um die Aktivität, Selektivität und Strukturänderungen während der Reaktion für die synthetisierten Katalysatoren zu untersuchen.

Ein monometallischer (Au_{25}), zwei bimetallische ($PtAu_{24}$ und Cu_xAu_{25-x}) und ein trimetallischer (Cu_xPtAu_{24-x}) Nanocluster wurden synthetisiert und auf CeO_2 stabilisiert, um sie als Katalysatoren für die WGSR einzusetzen. Kinetische Tests wurden durchgeführt, um einen Einblick in die Aktivitäts- und Selektivitätsunterschiede der verschiedenen Nanocluster-Katalysatoren zu erhalten. Die kinetischen Tests zeigten, dass die dotierten bi- und trimetallischen Katalysatoren die katalytische Aktivität für die Reaktion erhöhten. Dies führte zu einer höheren H_2-Produktion im Vergleich zum monometallischen Au_{25}-Nanocluster-Katalysator. Darüber hinaus zeigten die Ergebnisse der kinetischen Tests, dass die katalytische Aktivität auch vom eingesetzten Dotierungsatom abhängig war. Der bimetallische $PtAu_{24}$-Nanocluster-Katalysator zeigte die höchste CO-Umwandlung und produzierte das meiste H_2, gefolgt vom bimetallischen Cu-dotierten Cu_xAu_{24-x} Nanocluster Katalysator.

Diese Ergebnisse können durch die unterschiedliche Geometrie und Position des Dotieratoms der einzelnen Nanocluster, der Änderungen in der Clusterstruktur während der Reaktion und den unterschiedlichen CO-Adsorptionsstellen erklärt werden. Die Ergebnisse aus Operando-IR-DRIFT-Messungen der Katalysatoren stimmen letztendlich auch mit XAFS- und EXAFS Messungen überein, die zuvor auch von der Gruppe durchgeführt wurden. Die Forschungsergebnisse zeigen, dass für den $PtAu_{24}$-Katalysator das Pt-Atom, das sich ursprünglich auf der Innenseite des Clusters befindet, an die Oberfläche wandert und als isoliertes Atom eine stabile Position auf der Katalysatoroberfläche findet.

Die Kernclusterstruktur aus Gold wirkt dann als stabilisierendes Gerüst. Für den Nanocluster-Katalysator Cu_xAu_{24-x} konnte die Bildung von stabilen metallischen Cu-Cu-Bindungen, sogenannten "Inseln", auf der Oberfläche des Clusters beobachtet werden. Für den trimetallischen Cu_xAu_{24-x}-Katalysator wurde beobachtet, dass Cu-Atome während der Reaktion Pt-Cu- und Cu-Au-Bindungsstellen bildeten, was zu einer verringerten Effizienz im Vergleich zu, der von bimetallischen Katalysatoren führte.

Die Verwendung von bimetallischen Nanocluster-Katalysatoren führte zu einer Verbesserung der CO-Umwandlungsrate und der H_2-Erzeugung und die Katalysatoren behielten ihre Stabilität auch nach mehreren Läufen der WGSR bei. Diese Erkenntnisse verbessern das Verständnis der auf CeO_2 stabilisierten und dotierten Nanoclustern, was für die Entwicklung und Verwendung von derartigen Katalysatoren in der Zukunft wichtig ist. Nanocluster-Katalysatoren können nicht nur mit unterschiedlichen Metallatomen, unterschiedlicher Atomanzahl, unterschiedlichen Dotieratomen und unterschiedlichem Trägermaterial entworfen werden, sondern auch zur Verbesserung anderer Reaktionen eingesetzt werden.

Abstract

Since H_2 has become of interest as a promising fuel source, some research has shifted to find an efficient way to produce H_2 with the water gas shift reaction (WGSR), through the efficient design of a suitable catalysts. To allow the creation of an effective catalyst, a lot of work and research is put into the design. An understanding of the catalyst structure at the atomic level, as well as the processes that occur during the reaction, is required. Therefore, the aim of this work was to design different catalysts for the WGSR and test them with various methods to investigate the activity, selectivity, and structural changes during the reaction.

One monometallic (Au_{25}), two bimetallic ($PtAu_{24}$ and Cu_xAu_{25-x}) and one trimetallic (Cu_xPtAu_{24-x}) nanoclusters were synthesised and supported on CeO_2 to create catalysts for the WGSR. Kinetic tests were performed to have insight into the differences in activity and selectivity. The kinetic tests showed that the doped bi- and trimetallic catalysts increased the catalytic activity for the reaction, which resulted in a higher H_2 production in comparison with the monometallic Au_{25} nanocluster catalyst. Furthermore, the results of the kinetic tests demonstrated that the catalytic activity was also dependent on the dopant atom itself. The bimetallic $PtAu_{24}$ nanocluster catalyst exhibited the highest CO conversion and produced the most H_2, followed by the bimetallic Cu doped Cu_xAu_{24-x} nanocluster catalyst.

These results can be explained by the distinct geometries and position of the dopant atom of the individual clusters, changes in the cluster structure during the reaction, and variations in the CO adsorption binding sites. Furthermore, this is also in agreement with the results obtained from operando IR DRIFT studies of the catalysts and X-ray Absorption Fine Structure (XAFS) and Extended X-ray Absorption Fine Structure (EXAFS) measurements which were previously performed by the group. Research results show that for the $PtAu_{24}$ catalyst the Pt atom, originally located on the inside of the cluster, is migrating to the surface and finds a stable position as an isolated atom on the catalyst surface. The core cluster structure of gold then acts as a stabilizing framework. For the Cu_xAu_{24-x} nanocluster catalyst, the formation of stable metallic Cu-Cu bonds, so called "islands", on the surface of the cluster could be observed.

For the trimetallic Cu_xAu_{24-x} catalyst it was observed that Cu atoms formed Pt-Cu and Cu-Au bonding sites during the reaction, resulting in a decreased efficiency compared to that of bimetallic catalysts.

The utilization of bimetallic nanocluster catalysts resulted in an improvement of the CO conversion rate and H_2 generation and maintained their stability after several runs in the WGSR. These findings improved the understanding of doped nanocluster dynamics supported on CeO_2, which is important for the development and use of doped nanocluster catalysts in the future. Nanocluster catalysts can not only be designed with different metal atoms, different atom number, different dopant atoms and different support, but can also be used to improve other reactions.

Acknowledgement

The first thing I would like to do is thank Dr. Noelia Barrabes for supervising my master thesis. I am also grateful for being able to do my thesis in her amazing group. Thank you for the support, guidance, opportunities, and everything else you taught me during this time.

A special thanks to everyone in the ClusCAT group for the enjoyable time, help and support I had there.

I also want to thank my parents, family, friends and my partner for all their patience during the last years.

Contents

List of Figures

List of Tables

List of abbreviations

Acronyms

EXAFS	Extended X-ray Absorption Fine Structure
HOMO	Highest Occupied Molecular Orbital
IR	Infrared
LUMO	Lowest Unoccupied Molecular Orbital
MALDI	Matrix–Assisted Laser–Desorption–Ionization
MS	Mass Spectroscopy
NC	Nanocluster
RT	Room temperature
SEC	Size Exclusion Chromatography
UV-Vis	Ultraviolet-Visible
WGSR	Water gas shift reaction
XANES	X-ray absorption near edge structure
XAFS	X-ray absorption fine structure XAS
X-ray Absorption Spectroscopy	
XPS	X-ray Photoelectron Spectroscopy

Chemicals

2-PET	2-Phenyl-ethanthiol
DCM	Dichlormethan
EDA	Ethylenediamine
EtOH	Ethanol
MeOH	Methanol
THF	Tetrahydrofuran
TOAB	Tetraoctylammonium bromide

Sample names

AuCe	$Au_{25}(SC_2H_4Ph)_{18}$ / CeO_2
CuAuCe	$Cu_xAu_{25-x}(SC_2H_4Ph)_{18}$ / CeO_2
PtAuCe	$PtAu_{24}(SC_2H_4Ph)_{18}$ / CeO_2
CuPtAuCe	$Cu_xPtAu_{24-x}(SC_2H_4Ph)_{18}$ / CeO_2

1 Introduction and motivation

In recent years, there has been a considerable increase in the demand for cleaner energy, prompting the research of renewable fuel sources.[1] Because of its high energy content and versatility as a fuel source, hydrogen (H_2) has emerged as a promising choice. The water-gas shift reaction (WGSR) is one of several reactions for the generation of (H_2).[2,3] Carbon monoxide (CO) and water (H_2O) vapor is converted into (H_2) and carbon dioxide (CO_2). The rate of reaction increases with rising temperature, but the chemical equilibrium becomes unfavourable, and the CO conversion and equilibrium constant therefore declines. For this reason, CO conversion and H_2 production becomes more efficient at lower temperatures, however, the kinetics are getting slower.[4] As a result, finding catalysts with high catalytic activity and selectivity at lower temperatures is crucial for allowing efficient and industrial-scale catalytic reactions. A substantial amount of research is devoted to the design of catalysts, and it is essential to understand how reactants interact with the catalyst surface for a successful catalyst design.[5,6,6] Understanding the basic structure of a catalyst at the atomic level is essential to improve and create new ones for the WGSR.

Ligand protected metal nanoclusters (NCs) are a novel category of functional nanomaterials that possess atomic precision and can have a well-defined molecular structure.[7–9] In latest research, employed bimetallic Au NCs on a CeO_2 substrate have demonstrated remarkable stability, catalytic activity, and, for example, a good CO conversion rate in CO oxidation reactions.[10–12] Metal NCs are composed of less than 100 atoms, which are held together by weak chemical interactions, giving them properties that are different from bulk structures. The use of clusters offers control of the number of atoms or size, the type of atom they are made of and a possible surface design for active sites. The clusters also provide an excellent chance for studies regarding size dependent characteristics, the atomic structure and how they correlate with the reaction progression.[12–14] For the WGSR the metal nanoparticles Au, Cu, Pd and Pt have already been employed in several studies for catalysis, so they can act as an active surface and have been used as dopant atoms for the NC catalysts.[15–19] Thiolate protected $Au_{25}(SC_2H_4Ph)_{18}$ NCs are advantageous for numerous researchers due to their characteristics. In contrast to other Au clusters, they exhibit a distinct stability, reactivity, are relatively simple to synthesize, and are easy to fictionalize.[20,21] The so-called thiol "staples", where one S atom links with

two Au atoms, can stabilize the metal atoms around the core further, and, in contrast to other stabilizing units, like carbon monoxide or selenolates for example,[22] it is possible for the cluster to be isolated and stored in powder form for a long period, before they can be dissolved again in solvent.[10,13,23,24]

The core of the $Au_{25}(SC_2H_4Ph)_{18}$ NCs consists of 13 inner Au atoms. One central Au atom in the middle and the surrounding Au_{12} in the form of an icosahedron that is held together by six -S-Au-S-Au-S- staples. These staples are positioned on opposite sides of the icosahedron.[25] The $Au_{25}(SC_2H_4Ph)_{18}$ NCs can also be doped with various metal atoms, however, it depends on the type of atom which place they will occupy within the cluster, while the cluster structure itself remains intact.[12,25] The introduction of metal atom doping can be utilized to modify the surface of the cluster to adjust to diverse conditions, thereby enhancing the catalytic activity of the catalyst. The stability and catalytic activity of gold nanoclusters can be enhanced by the introduction of hetero atom dopants such as Cu and Pt for example.[12] A Pt dopant atom can then be found in the centre of the Au NCs and the Cu dopant atoms around the core at the Au(I) thiolate staples.[10] As support materials for CO oxidation reaction reducible oxides have been found to be particularly effective, such as TiO_2, CeO_2, and SiO_2 for example. Studies have also shown that Au supported on CeO_2 resulted in a higher catalytic activity for catalysing low temperature WGSR, due to the support being a reducible oxide and taking an active part in the reaction.[12,16,18]

Therefore, this master thesis is set to investigate the synergistic effects between the metals of the dopant atoms Cu, Pt, and with Au_{25} on a CeO_2 support for the WGSR. Monometallic Au_{25}, bimetallic $PtAu_{24}$ Cu_xAu_{25-x} and trimetallic Cu_xPtAu_{24-x} NCs were synthesized and stabilized on the CeO_2 support. It is unclear which specific roles the dopant atoms hold in the catalysis of the WGSR and how the cluster geometry correlates to the catalytic activity. It has not yet been investigated for this catalyst system.[26,27] As a result, kinetic tests were performed to measure the catalytic activity, selectivity, stability, and CO conversion rate of the synthesized catalysts. To gain a more precise understanding of the processes that occur during the reaction on the surface, operando IR DRIFT measurements were also performed. The mixing of several metals in bimetallic or trimetallic NCs has the potential to exhibit synergistic effects, resulting in an increase in catalytic activity.

Furthermore, moving forward some cluster characteristics may be further fine-tuned by changing the number of atoms, cluster size, different doping atoms, other metals, ligands, and the support material. Ultimately, exploring the WGSR for hydrogen production can not only provide valuable insights into ways to improve efficiency and sustainability, but it also provides a powerful method for cleaning industrial exhaust gas. Furthermore, doped NCs catalysts can also be used for other reactions. Therefore, it is crucial to control and understand the active sites at an atomic level to ensure a good catalyst design.

2 Theoretical backgrounds

2.1 Water–gas shift reaction

Although hydrogen is an energetic fuel, it does not naturally occur in its free form, and must therefore be produced by utilizing other energy sources, making it a secondary energy source.[2] As the world progresses towards a hydrogen economy, the WGSR became an important intermediate step in carbon-based hydrogen generation. It is used for hydrogen enrichment and CO reduction in synthesis gas. In a WGSR, CO reacts with H_2O vapor to produce CO_2 and H_2.[3,4] The chemical equation can be seen in equation 1.

$$H_2O + CO \rightleftarrows H_2 + CO_2 \tag{1}$$

The WGSR is both, moderately exothermic and reversible. It produces energy with a reaction enthalpy of -41.2 kJ/mol.[4] As the temperature increases, the equilibrium constant of the reaction decreases. During low temperatures, the reaction is thermodynamically favoured, while at high temperatures, it is kinetically favoured. Which means that with increasing temperature, the chemical equilibrium shifts from the products to the educts.[4] Two mechanisms have been suggested for the WGSR. A redox mechanism and an associative Langmuir-Hinshelwood mechanism. The actual process, however, is still uncertain and varies on whether the reaction is researched at lower or higher temperatures and if a catalyst is present.[28]

2.2 Catalysis and catalysts

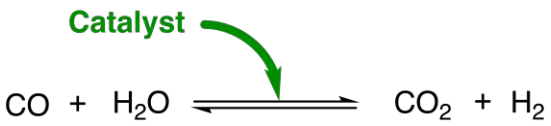

Figure 1: Catalysis of the WGSR with a catalyst.

2.2.1 General information

In chemistry, catalysis describes the process which involves a substance, the catalyst, that affects the products or rate of a reaction (Figure 1).[29] Chemical reactions can therefore be accelerated with the use of a catalyst, by increasing the rate at which the reaction takes

place. As a result of catalyst-reactant interactions, intermediate products are formed that eventually result in the final products of the reaction. A catalyst is ideally not consumed in a reaction and remains unchanged afterwards. Several factors affect the reaction rate, including the amount (or size), type, age, and active surface area of the catalyst, as well as operation temperature and pressure.[29] A high-performance catalyst for example, allows chemical reactions to take place faster with then ideally resulting in a cheaper and selective generation of the desired product. The catalyst should therefore have the potential to use reagents more efficiently, increase the yield, avoid by-products, reduce waste, and result in an overall reduction of energy consumption during the reaction. Research on catalysis and catalysts is, therefore, crucial to maximizing the efficiency of all resources.[4] An uncatalyzed reaction does not follow the same reaction path (or reaction coordinate) as a catalysed reaction with catalyst. With a catalyst, the reaction proceeds through a reaction path that requires less energy to transform the educts into the products. As a result, because the reactants now have the necessary energy to pass through an energy maximum that requires less energy for activation, then, more molecule collisions can reach the "transition state".[30] The transition state represents an intermediate state that the reactants transform into before eventually becoming the final product. During a chemical reaction, the transition state is determined by a certain configuration along the reaction coordinate, which represents the reaction pathway in an abstract, one-dimensional nature. It corresponds to the state with the highest potential energy along the reaction coordinate. Therefore, the molecule must overcome this energy barrier to form the product. However, catalysts have the ability to enable reactions that might otherwise be hindered by kinetic barriers, or a too high activation energy.[31] The catalyst is able to boost the speed or selectivity of a reaction, or it can allow the reaction to take place at lower temperatures.[4,31] An energy profile diagram can be used to depict this impact, which can be seen in Figure 2.

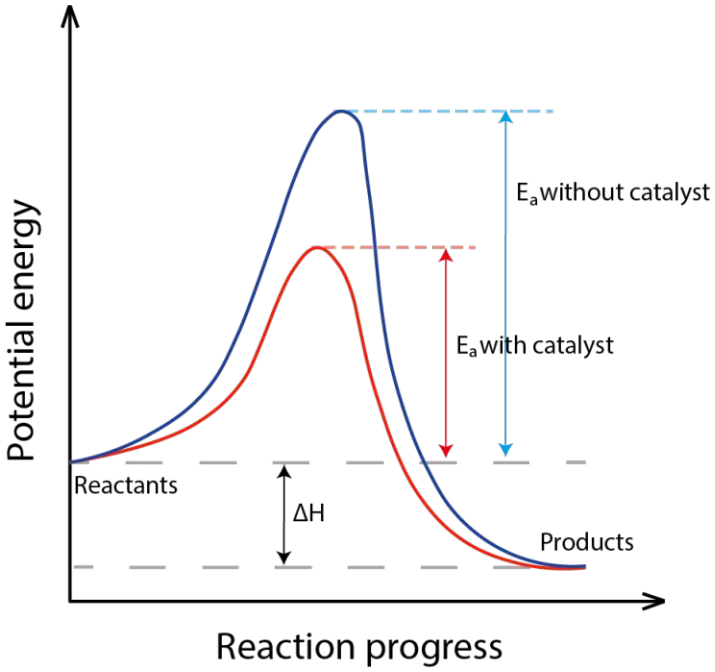

Figure 2: Activation energy profile diagram of a reaction with (red) and without (blue) catalyst with the overall energy input to a chemical system as it moves from reactants to products.

As can be seen in Figure 2, the activation energy E_a is lower when a catalyst is being used for a reaction. A lower activation energy allows a greater fraction of collisions to occur. As a result, higher activation energies correlate to slower reactions and lower activation energies to faster reactions. Exothermic reactions are often associated with low activation energy, whereas endothermic reactions are often associated with high activation energy. By offering an alternate, lower activation energy pathway, the catalyst promotes the transition between reactants and products. The catalyst only influences the kinetics of a process, not its thermodynamic properties.[32]

2.2.2 Heterogeneous catalysis

Catalysis can be categorized into three main groups: homogeneous catalysis, heterogeneous catalysis, or bio-catalysis. Proteins or nucleic acids that catalyse activities outside of live cells are known as biocatalysts. The components of catalyst in homogeneous catalysis are dispersed in the same phase as the reactant (usually gaseous or liquid), while the components of a catalyst in heterogeneous catalysis is not. In heterogeneous catalysis, solid phase catalysts and gas phase reactants are commonly used.[32,33] Since the emphasis of this thesis is heterogeneous catalysis the next chapters will only focus on this area

of subject. Heterogeneous catalysis is critical for efficient large-scale chemical syntheses, as well as controlled product generation. It is an effective method for increasing the efficiency and sustainability of chemical processes. This method employs solid catalysts, such as metals or metal oxides, as reaction surfaces.[34] The reactants bind to the surface, an active surface site of the catalyst, then will undergo a chemical transformation, and then release the products (Figure 4).

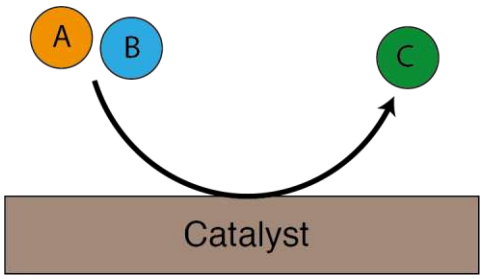

Figure 3: Two reactants A and B in gaseous form react with the help of a solid catalyst to form product C.

The adsorption can be divided into the two types physisorption and chemisorption. When a molecule is attracted to a surface by weak forces like van der Waals forces, it is referred to as physisorption. There is no chemical bond formed, and the adsorbate (adsorbing molecule) and adsorbents (substrate where molecule adsorbs) electronic states remains unchanged. The energies range from 3 to 10 kcal/mol. Chemisorption takes place when a molecule comes near enough to the surface for chemical bonds to form, with energies generally ranging from 20 to 100 kcal/mol.[35,36] Surface reactions are characterized by three major mechanisms that can be seen schematically in Figure 4.

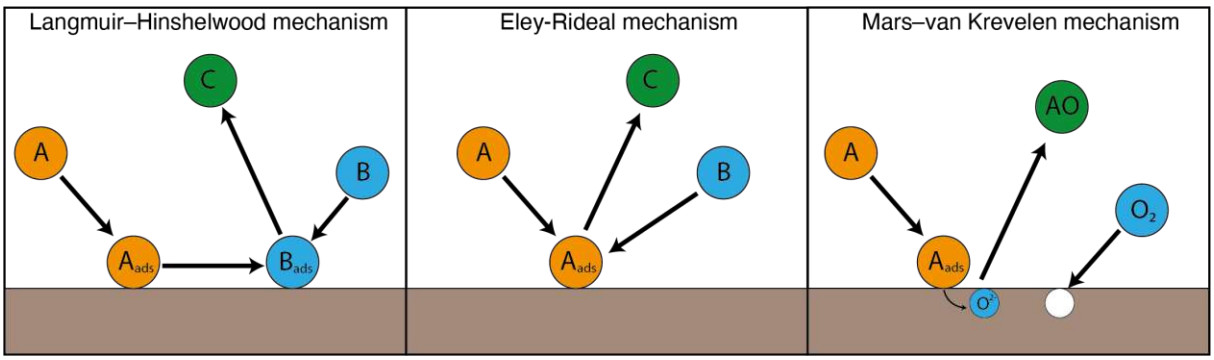

Figure 4: Schematic representation of the different adsorption mechanisms (Langmuir-Hinshelwood, Eley-Rideal and Mars-van Krevelen).

The Langmuir-Hinshelwood mechanism occurs when both reactants, for example A and B, adsorb onto the active surface sites to create product C, and then the product desorbs again. The Eley-Rideal process occurs when just one reactant, A, adsorbs onto the surface and reacts with non-adsorbed reactant B to create product C, which is then desorbed.[37] The Mars-van Krevelen process is a catalytic reaction mechanism in which reactant A is adsorbed from the gas phase onto the surface, oxidized with lattice oxygen, desorbed as product AO, and then re-oxidizes to replace oxygen vacancies.[38] Most heterogeneously catalysed reactions can be described by the Langmuir-Hinshelwood model. Among the primary advantages of heterogeneous catalysis can be attributed to the solid nature of the catalysts and the possibility for the composition and surface structure to be precisely designed. The endless potential makes it accessible for various applications in chemical synthesis and promotes the development of new technologies.[37]

2.2.3 Nanocatalysis with metal NCs

Nanocatalysis is an area of research that focuses on the use of nanomaterials that are precisely defined, usually with a size of less than 100 nm, and are used in catalysis. Tiny metal NCs with less than 200 atoms belongs to the class of nanomaterials which can be used for nanocatalysis. Metal NCs hold importance due to their precise atomic structures, attractive properties, and broad possibilities for utilization across diverse fields. They have a high surface-area-to-volume ratio and the properties of the NCs differs greatly from bulk structures. This is due to an orbital overlapping between metal atoms in cluster structures.[39,40] A schematic representation for the electronic structure of different materials with different particle numbers can be seen in Figure 5.

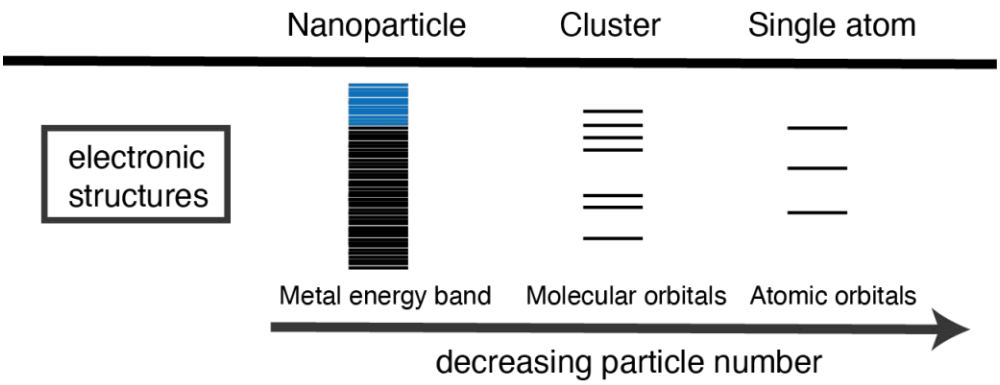

Figure 5: Schematic representation of the electronic structure of material with different particle numbers.

Each atoms electron orbital forms a unit with delocalized electrons and then contributes to the electronic structure. The density of states is influenced by the number of atoms present. For larger NCs, a continuous energy level will form, since the bandgap between Highest Occupied Molecular Orbital (HOMO) and Lowest Unoccupied Molecular Orbital (LUMO) becomes smaller. The combination of several atoms results in continuous bands in bulk structures. With a decreasing number of atoms, the band continuously transforms into disconnected energy levels. Therefore, the cluster size is also crucial to the catalytic abilities of the material and needs to be controlled during the synthesis.[39,40] In order to stabilize metal clusters during synthesis, organic ligands including thiols, acetylene, carbines, phosphines, or selenolates can be used. They change the cluster's electronic states in addition to stabilizing it.[41–43]

Within this thesis, the focus lies on thiolate protected NCs, due their simple synthesis and already well researched properties, like, robust sulphur-metal interactions, solution stability and possibility to functionalize NCs.[41,44] For some reactions, like an alcohol oxidation for example, a decrease in activity or even a full inhibition is reported, when thiol ligands are present.[45] Although, for other reactions, like the semi hydrogenation of alkynes for example, it is possible for ligands to enhance the selectivity and catalytic activity.[46] Au NCs are suited for catalytic applications due to their distinctive geometric and electrical characteristics. Thiolate Au NCs can be produced easily with either monodisperse or polydisperse size distribution, and an easy size control is possible during synthesis. Some studies concluded that they act as suitable catalysts for the low temperature CO oxidation, when supported on an oxide.[7,47,48] The geometry of thiolate protected Au NCs also relies

on the atom number, and only clusters where the variables m and n have a particular value in the chemical formula $Au_m(SR)_n$, are considered thermodynamically stable. For the synthesis, regulating the reaction temperature and aggregation conditions for the $[Au(I)-SR]_x$ polymeric intermediate is important. A thiol excess of 3:1 (compared to gold) is necessary, to convert Au^{III} into $Au^{I}-SR$ polymers. Then, 10 equivalents per mole of gold of a reducing agent, like $NaBH_4$, is needed to convert Au^{I} to Au^{0}. It is possible, that $Au_{25}(SC_2H_4Ph)_{18}$ clusters can be synthesised with a high yield and high purity.[20,41] $Au_{25}(SC_2H_4Ph)_{18}$ NCs have a core structure of 13 inner Au atoms, with one central Au atom in the middle (Figure 6). Au_{12} are surrounding the core in the form of an icosahedron (Figure 7) that is held together by six -S-Au-S-Au-S- staples, positioned on opposite sides of the structure, with in total 18 thiolate ligands (Figure 8). The NCs have a D_{2h} like symmetry.[25,25,27,41,49]

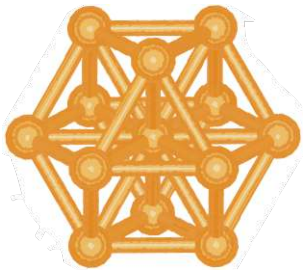

Figure 6: Schematic cluster structure of the Au_{13} core.

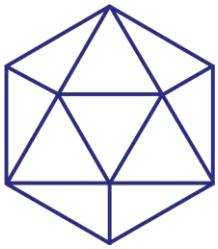

Figure 7: Form of the Au_{12} and thiolate icosahedron which surrounds the Au_{13} core.

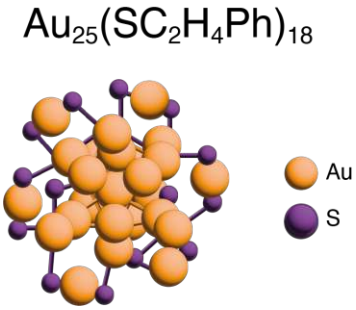

Figure 8: Schematic representation of the $Au_{25}(SC_2H_4Ph)_{18}$ NCs.

2.2.4 Doping effect

Doping describes the exchange of one to more Au atoms for those of another metal like Pd, Pt, Cu, or others. It has a significant effect on the NC properties (reactivity, stability, electronic structure) and effects catalytic activity. Doping can also considerably enhance the catalytic capabilities of the NCs, which was demonstrated by earlier studies.[50,51] The nature of the dopant atom significantly affects the properties and geometry of doped Au_{25} clusters, like M_1Au_{24} (M = Pd, Pt). A Pt dopant atom can be found in the centre of the Au NC and the Cu dopant atoms outside at the Au(I) thiolate staples (Figure 9).[10,50] In comparison to pure gold NCs and NCs with Ag or Cu doping, Pd- or Pt-doped NCs demonstrate more stability. The lower stability of Cu-doped Au NCs has been attributed to the location of the dopant atom inside the cluster structure for example.[15–19,51] There is still plenty of research being conducted, that deals with uncertainties of the complex interaction of the dopant atoms with cluster structure, support, and more, which is yet not completely understood. Only a small number of doped clusters have had their structures completely uncovered, and the synergistic effects between one to several dopant atoms during the reaction is still unclear.

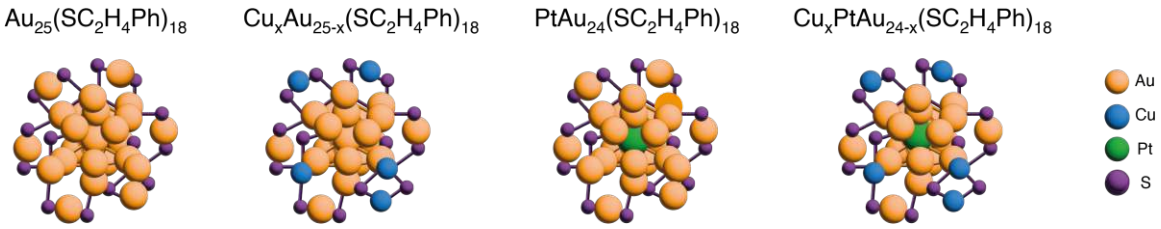

Figure 9: Schematic representation of mono-, bi- and trimetallic doped $Au_{25}(SC_2H_4Ph)_{18}$ NCs.

2.2.5 Support and loading effect

Au NC catalysts are included in the category of heterogeneous catalysts since they are stabilized on a support. They offer great stability for the cluster, can increase catalytic activity, and can help to avoid sintering. Au NCs have been tested on a variety of solid supports, including oxides and carbon for example. It has been demonstrated that the type of support material can have a significant impact on the catalytic activity of supported Au NCs. The support material can be selected according to reaction condition

and other requirements. The materials can be roughly divided into two groups, depending on how the support interacts with the cluster: active/reducible and irreducible/inert[41,52] Previous studies have shown that the cluster structure has stronger interactions with reducible supports, like TiO_2 and CeO_2, which boost the catalytic activity of Au_{25} cluster catalyst in oxidation reactions. Yet, the catalytic activity for Au_{25} supported on CeO_2 is higher as on TiO_2 for a low temperature CO oxidation, probably due to the charge distribution and electron transfer of Au_{25} on the CeO_2 support material.[47] CeO_2 also proved to be an appropriate support material for the WGSR.[3,26] H_2O vapor is activated on the oxygen vacancies on the CeO_2 surface. The reaction takes place at the metal-CeO_2 interface after CO is adsorbed on the metal nanoparticles.[26,53] Since the clusters need to be dispersed on the surface for the formation of active sites, the relative loading of the clusters (in wt.% relative to amount of support) needs to be taken into account too. The amount of cluster on the support needs to be considered during catalyst synthesis, since a too high cluster load can lead to a decreased catalytic activity, likely due to confinement of the clusters in the support material. Previously performed research tested the optimal load for Au_{25} NCs, which revealed that a loading between 0.04 and 1.07 wt.% resulted in an average particle size of 1.9 $\pm$ 0.6 nm and 1.8 $\pm$ 0.5 nm, and helped preserve the average particle size, in contrast to a higher cluster loading.[41,54]

2.2.6 Pretreatment effect

According to earlier wort by Yin et al.,[55] the catalytic activity can be heavily influenced by the stabilizing ligands. The group suggested that the cluster structure is too bulky and can prevent the CO from adsorbing to the active Au sites on the surface.[55] Therefore, pretreatment that would remove the ligand shells were suggested. The sulphur of the thiolate ligands for example, were catalyst poison and block active Au sites. Despite several studies on various cluster pretreatment, there are still numerous discrepancies and uncertainties within the research community.[7] Some research shows that a partial removal of the ligands led to a higher activity of the NC catalysts, rather than a complete ligand removal.[47,48] Other researchers, who tested pretreatments have found that for some NC catalysts, like ones that are based on an Au_{144} structure, already demonstrate a good catalytic activity without ligand removal.[56] However, this is not the case for Au_{25} NC catalysts, probably due to their long stables of -SR-Au-SR-Au-SR- groups, which is less

stable. During pretreatment and reaction, the originally well-defined Au cluster structure can collapse, which is also influenced by the original cluster size and support material.[7,52] Various pretreatment for $Au_{25}(SC_2H_4Ph)_{18}$ based clusters was previously tested by Garcia et al.[12] based on previous studies by Li et al.[56] The reported pretreatments (conditions can be found in chapter 3.5.1) showed to have a significant effect on the catalyst activation. While the pretO_2 oxidation is used to remove pollution and residue from the surface of the catalyst and remove ligands that are there from the syntheses, the pretH_2 reduction allows the reduction of oxidized noble metals like Pd and Au for example.[7,52]

3 Experimental

The additional information of the mentioned chemicals can be found in the Appendix in Table A1.

3.1 Cluster synthesis

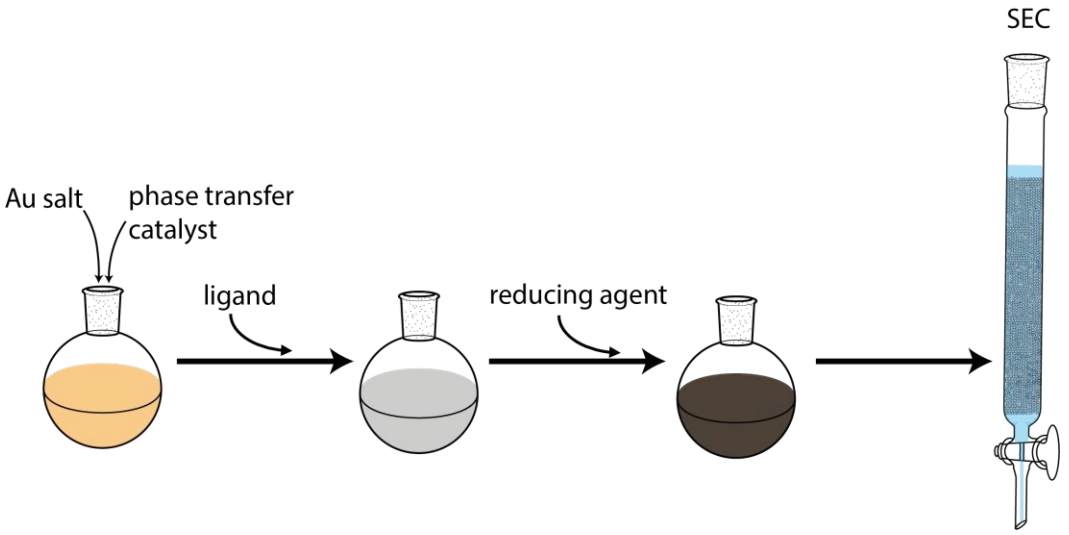

Figure 10: Overview of the cluster synthesis steps and purification with a chromatography.

3.1.1 $Au_{25}(SC_2H_4Ph)_{18}$

The synthesis was conducted using a modified synthesis protocol by Truttmann et al.[57] and Shivhare et al.[58] An amount of 50 ml tetrahydrofuran (THF) and 1.27 mmol of $HAuCl_4 \cdot 3\,H_2O$ were mixed with 1.52 mmol of tetraoctylammonium bromide (TOAB) and stirred for 10 minutes at room temperature (RT) resulting in a yellow-orange solution. Then, 0.85 mL of 2-Phenyl-ethanthiol (2-PET) (=$(SC_2H_4Ph)_{18}$) were added to the solution and stirred until it became transparent. 12.97 mmol of $NaBH_4$ in 10 ml of ice-cold distilled H_2O was added rapidly, leading to a dark brown reaction mixture. The solution was stirred for 3 days at RT, then the solvent was evaporated with a rotary evaporator and the oily orange product was washed first with methanol (MeOH) and then dichlormethan (DCM). This ensured that unwanted by-products were eliminated. The resulting orange DCM solution was reduced again with the rotary evaporator (Buchi Rotavapor R-210). The remaining viscous orange product was washed three times with MeOH. The obtained precipitation was dissolved in DCM, filtered, and evaporated.

The clusters were then separated by Size Exclusion Chromatography (SEC) and their purity evaluated by Ultraviolet-Visible (UV-Vis) spectroscopy and matrix-assisted laser desorption ionization mass spectrometry (MALDI-MS).

3.1.2 $Cu_xAu_{25-x}(SC_2H_4Ph)_{18}$

The clusters were prepared according to a procedure presented by the Negishi group.[59] A solution of 0.48 mmol $HAuCl_4 \cdot 3\,H_2O$ was mixed with 0.12 mmol $CuCl_2 \cdot 2\,H_2O$ and 0.66 mmol TOAB which was then dissolved in 50 mL of MeOH. The red solution was stirred at RT for 15 minutes. Next 0.96 mL of 2-PET was added to the mixture, which resulted in a grey precipitate and was stirred for another 15 minutes at RT. The reaction mixture was then reduced with 6 mmol (NaBH4) dissolved in 10 mL of ice-cold distilled H_2O, turning the solution black, and further stirred for 3 hours at RT. Subsequently, the solvent was removed by evaporation and the product washed twice with MeOH and dried again. The product was extracted with acetonitrile and dried again. The clusters were further purified with a SEC and analysed by UV-Vis and MALDI-MS.

3.1.3 $PtAu_{24}(SC_2H_4Ph)_{18}$

The clusters were prepared according to a procedure published by Sels et al.[60] First, 0.43 mmol $H_2PtCl_6 \cdot 6\,H_2O$ and 0.02 mmol TOAB were mixed with 0.36 mmol of $HAuCl_4 \cdot 3\,H_2O$ solution and 60 mL of THF and stirred for 30 minutes, resulting in a light-yellow solution. Then 0.69 mL of 2-PET were added turning the solution orange and stirred for another 10 minutes. Next, the mixture was reduced with 20.60 mmol $NaBH_4$, dissolved in 10 mL ice-cold distilled H_2O, turning the solution dark brown. The solution was stirred for another 4 hours, after which the solvent was removed with the rotary evaporator and the precipitate was washed 3 times with MeOH, then acetonitrile and lastly acetone. The product was then dissolved in DCM and dried, then again in THF, filtered through a syringe filter and dried. The clusters were further purified with a SEC and analysed by UV-Vis and MALDI-MS.

3.1.4 $Cu_xPtAu_{24-x}(SC_2H_4Ph)_{18}$

For the generation of the trimetallic cluster a prepared Cu-ligand was mixed with the previously synthesized Pt-cluster. The Cu-ligand was prepared with the combination of two solutions (Solution A and Solution B). For Solution A, 0.36 mmol of $CuCl_2 \cdot 2\,H_2O$ was combined with 1 mL of distilled H_2O and 5 mL of MeOH. The mixture was stirred until the colour turned green. Then 0.60 mL of 2-PET, 7 mL of EtOH, and 2 mL of ethylenediamine were mixed. The two solutions were then homogenized and stirred until a light turquoise solid was produced resulting in the Cu-ligand. 0.20 μmol of the Pt-cluster is then dissolved in 5 mL of toluene. The deep green liquid is then mixed with 4.10 mg of the previously produced Cu-ligand, resulting in a cloudy solution. After stirring for 20 minutes, the reducing agent $NaBH_4$ is added, and the liquid was stirred again. The solvent is then removed under reduced pressure. The clusters were further purified with a SEC and analysed by UV-Vis and MALDI-MS.

3.1.5 SEC

To remove the excess of thiol ligands from the clusters the further purification of the clusters is crucial for a correct catalyst research. The synthesized polydisperse clusters can be separated depending on their size with a SEC. With the SEC the smaller NCs have a longer eluation time due to them being stuck in the pores of the stationary phase, while the bigger NCs have a faster eluation time, which separates them into different fractions. To see which fractions, hold which NC size, they are further analysed with UV-Vis spectroscopy. SX1 bio-beads from Biorad with a particle size between 40 - 80 μm were used as stationary phase. As the eluent THF was used for the isolation of the NCs.

3.2 Cluster characterisation

3.2.1 UV-Vis spectroscopy

The UV-Vis spectra of the nanoclusters, which were dissolved in DCM, were recorded on a VWR UV-1600PC UV-Vis spectrometer.

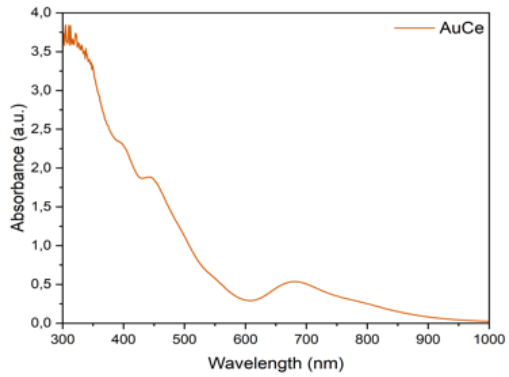

Figure 11: UV-Vis spectrum for $Au_{25}(SC_2H_4Ph)_{18}$ NCs.

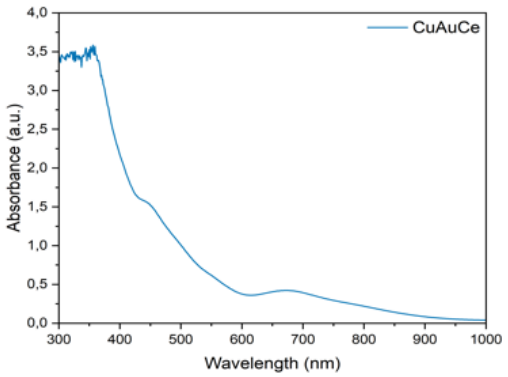

Figure 12: UV-Vis spectrum for $Cu_xAu_{25-x}(SC_2H_4Ph)_{18}$ NCs.

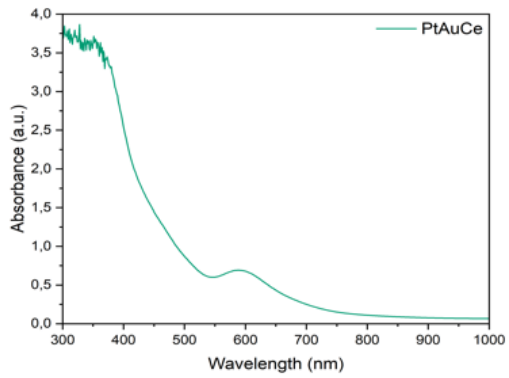

Figure 13: UV-Vis spectrum for $PtAu_{24}(SC_2H_4Ph)_{18}$ NCs.

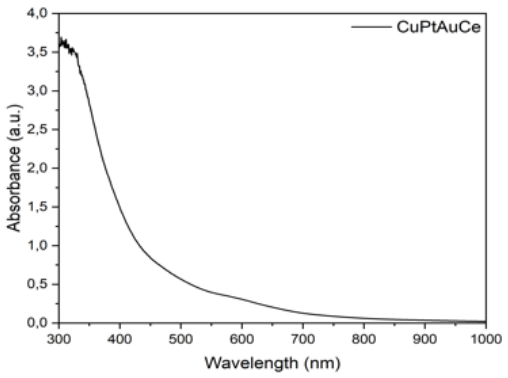

Figure 14: UV-Vis spectrum for $Cu_xPtAu_{24-x}(SC_2H_4Ph)_{18}$ NCs.

3.2.2 MALDI

An RTOF mass spectrometer from Shimadzu was used to conduct the MALDI-MS measurements and 2,4,6-Trihydroxyacetophenone was used as the MALDI-MS matrix. To produce mass spectra of sufficient resolution [3000-5000, full width half-maximum (fwhm)], MALDI-RTOF-MS were used near the boundary laser intensity. Every mass spectrum consisted of an average of 300–600 single and not selected laser pulses (lambda = 337 nm at 50 Hz). Due to high fragmentation, no MALDI spectrum of the $Cu_xAu_{25-x}(SC_2H_4Ph)_{18}$ cluster could be recorded. The trimetallic $Cu_xPtAu_{24-x}(SC_2H_4Ph)_{18}$ cluster showed a high fragmentation. For this reason, the variable x is used for the Cu amount in the clusters since this cluster still have a size distribution and are not monodisperse.

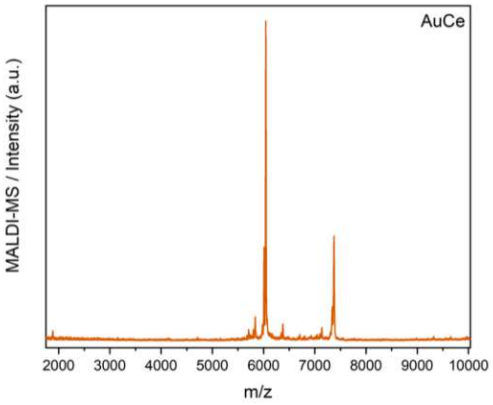

Figure 15: MALDI-MS spectrum for $Au_{25}(SC_2H_4Ph)_{18}$ NCs.

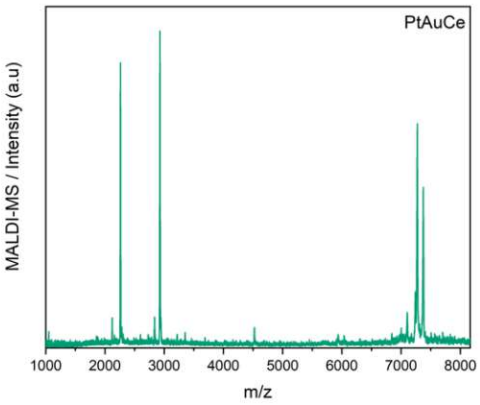

Figure 16: MALDI-MS spectra for $PtAu_{24}(SC_2H_4Ph)_{18}$ NCs.

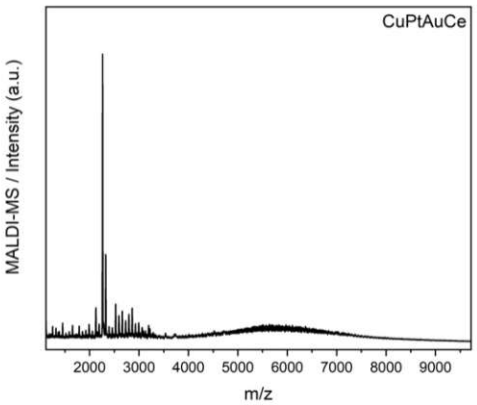

Figure 17: MALDI-MS spectra for $Cu_xPtAu_{24-x}(SC_2H_4Ph)_{18}$ NCs.

3.3 Catalyst preparation

The Au mono-, bi- and trimetallic nanoclusters were then supported on CeO_2 (Alfa Aesar, 15-30 nm particle size, 30-50 m^2/g surface area) using a wet impregnation (Figure 18).[61]

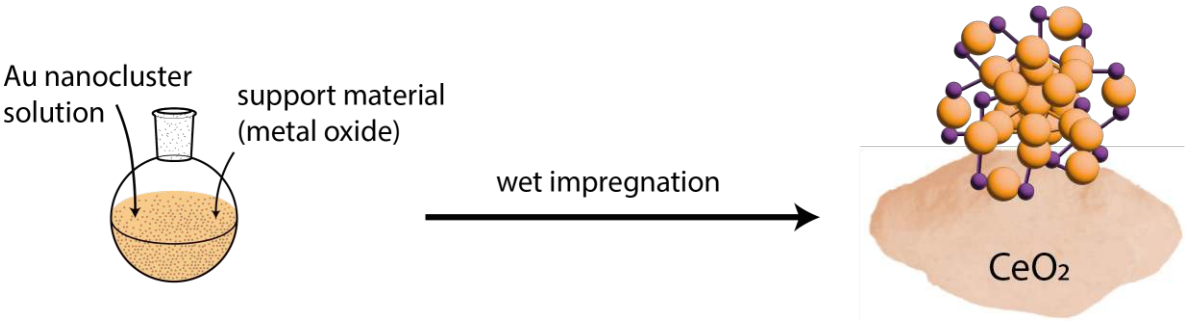

Figure 18: Overview of the cluster synthesis steps and purification with a chromatography.

For the preparation of the catalysts with a theoretical amount of 0.5 $wt.\%$ of cluster, the clusters were dissolved in toluene and added dropwise to a stirred suspension of ceria oxide in toluene. After complete addition, stirring at RT was continued for 24 h. The supported clusters were then separated from the solution by filtration and washed with MeOH, the powder dried under reduced pressure. In total four different types of catalysts were synthesized according to Table 1.

Table 1: Chemical formulas of the created catalysts and their abbreviations.

Catalyst	**Type**	**Abbreviation**
$Au_{25}(SC_2H_4Ph)_{18}$ / CeO_2	monometallic	AuCe
$Cu_xAu_{25-x}(SC_2H_4Ph)_{18}$ / CeO_2	bimetallic	CuAuCe
$PtAu_{24}(SC_2H_4Ph)_{18}$ / CeO_2	bimetallic	PtAuCe
$Cu_xPtAu_{24-x}(SC_2H_4Ph)_{18}$ / CeO_2	trimetallic	CuPtAuCe

3.4 Catalyst characterisation with TXRF

The exact metal loading in wt.% of the gold nanocluster catalysts was determined by total X-ray fluorescence spectroscopy (TXRF), using an ATOMIKA 8030C X-ray fluorescence analyzer. The samples were measured with Mo-Ka as the X-ray source at ambient conditions and in total reflection geometry. Samples were attached to total reflecting quartz reflectors using 1 mg of the cluster catalyst sample mixed with 5 μL of poly-(vinyl alcohol) solution for fixation. To prevent cross contamination, blank measurements of the unloaded reflectors were taken before each measurement. Detection limits of the quantified elements are in the range of 10-100 μg. The method has an error of $\pm$ 10%. Pt values should be considered carefully, since the lines overlap with the Au lines a lot.

Table 2: Results of the TXRF measurements of the amount of cluster loading regarding the amount of CeO_2 in wt. %

Loadings related to CeO_2 amount in wt.%				
Sample	**Au**	**Pt**	**Cu**	**Total**
AuCe	0,58	x	x	0,58
PtAuCe	0,36	0,11	x	0,46
CuAuCe	0,26	x	0,06	0,32
CuPtAuCe	0,14	0,04	0,05	0,23

3.5 Kinetic tests

Catalytic activity studies of the nanocluster catalysts during the WGSR were performed using a flow reactor coupled to an online micro gas chromatograph (Micro-GC, Fusion 3000A, Inficon). Around 25 mg of catalyst was used for all experiments. The catalyst was placed between two glass wool plugs in a quartz glass tube, with a Ni/NiCr thermocouple submerged in the catalyst powder connected to a PID temperature controller (EMSR EUROTHERM GmbH) connected to an oven, the reactor. A Bronkhorst mass flow controller was also connected to the oven for the gas flow control. The setup can be seen in Figure 20.

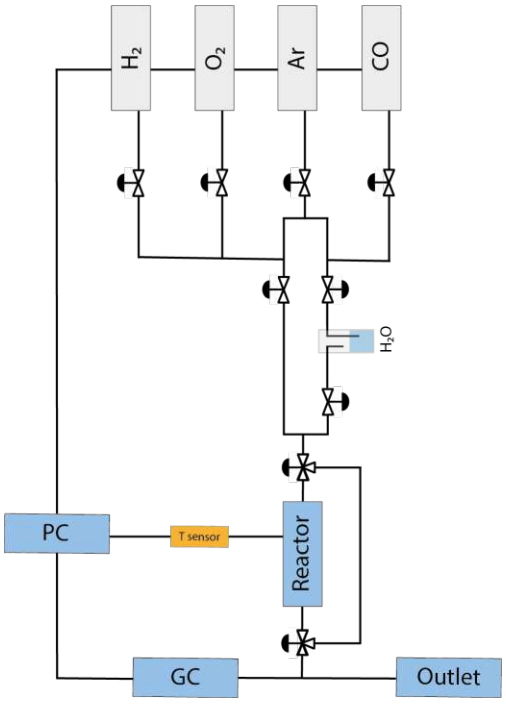

Figure 19: Set up of the reactor for the kinetic tests with gas supply from left to right: Hydrogen, Oxygen, Argon, Carbon monoxide.

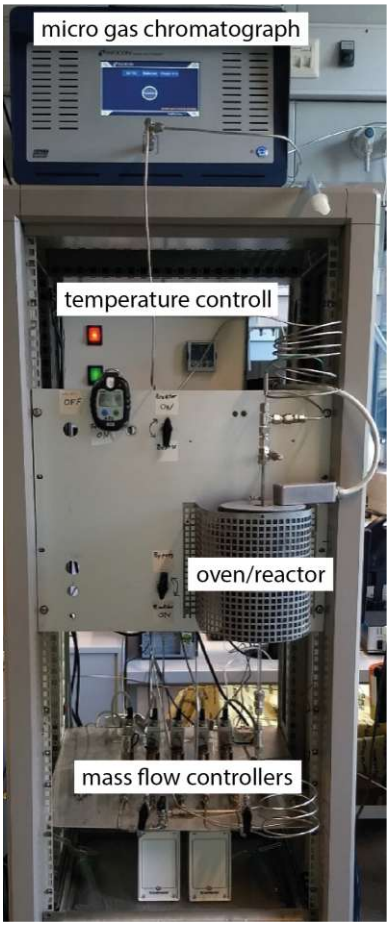

Figure 20: Image of the reactor set up for the catalytic activity tests.

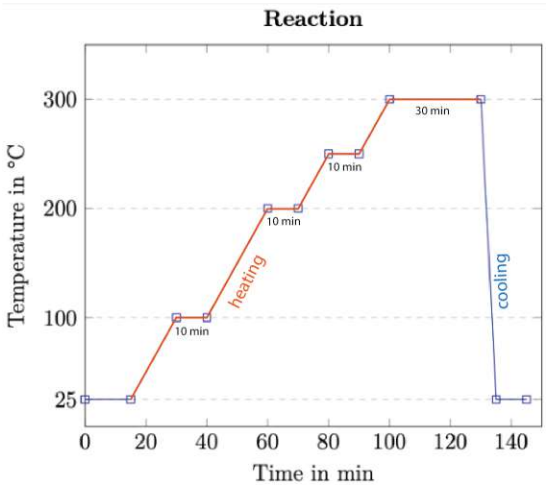

Figure 21: Heating scheme during the WGSR for the catalytic tests of the catalysts.

All catalysts were pretreated in an oxidative and reductive atmosphere. To compare the activity of the Au nanocluster catalysts, all data was normalized to the amount of catalyst used and the respective cluster loading of the TXRF measurement results of Table 2. The CO conversion was calculated with the measured area of CO according to equation 2. The equipment set up can be seen in Figure 19.

$$CO_{\,Conversion}\,(\%) = \frac{CO_{(T_0)} - CO_{(T_x)}}{CO_{(T_x)}} \tag{2}$$

3.5.1 Pretreatment conditions

Each catalyst would first undergo the oxidative pretreatment (pretO_2) with a gas flow of 5% O_2 in Ar (total gas flow of 20 ml/min) and a temperature ramp of 10°C/min up to 250°C. The maximum temperature was then maintained for 30 minutes before the sample was cooled to RT in Ar (20 ml/min). Then the catalyst would undergo the reductive pretreatment (pretH_2) with a gas flow of 5% H_2 in Ar (total gas flow of 20 ml/min) and a temperature ramp of 10°C/min up to 250°C. The maximum temperature was again maintained for 30 minutes before cooling the sample to RT in Ar (20 ml/min).

3.5.2 Reaction conditions

After the pretreatments the gas flow composition was then changed to reaction conditions (1% CO and 1.84% H_2O in Ar; 21 ml/min total gas flow) and held for 15 minutes at RT for equilibration. The temperature was then increased to 100°C, 200°C and 250°C with a ramp of 5°C/min and was held there for 10 min until the temperature was increased to 300°C with the same ramp and kept there for 30 min. Then the catalyst was cooled to RT under Argon (20 ml/min).

3.6 Operando IR DRIFT studies

In operando IR DRIFT studies were conducted using a Bruker Vertex 70 spectrometer. The MTC detector with a resolution of 4 cm^{-1} was cooled with liquid N_2. The catalyst was transferred into a DiffusIR flow cell from PIKE technologies with IR transmissible CaF_2 windows and connected to a Liquid Recirculator from PIKE Technologies (Figure 4.2). The gas flow was controlled with a MULTIGAS CONTROLLER 647C. IR spectra were recorded in a 3-minute interval with an average of 256 scans.

Figure 22: Image of the set up for the operando IR DRIFT studies.

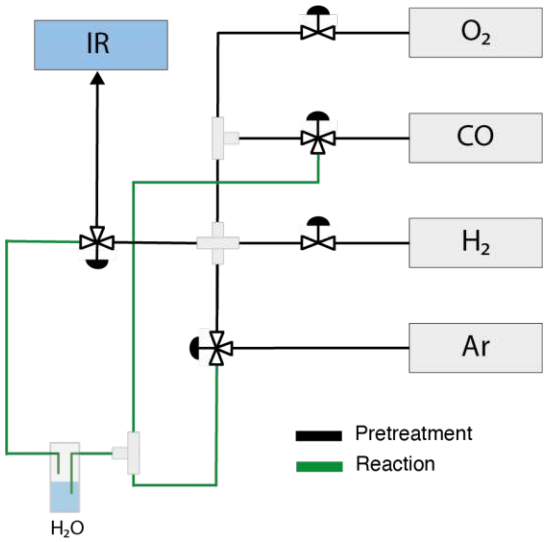

Figure 23: Set up of the equipment for the operando IR DRIFT studies with gas supply from top to bottom: Oxygen, Carbon monoxide, Hydrogen, Argon.

3.6.1 Pretreatment conditions

The sample was heated as described before in chapter 3.5.1 while simultaneously recording the IR spectra (MIR, resolution 4 cm^{-1}). The gas flow was reduced, to make sure that the sample would not move while the spectra where recording. The system was flushed with a flow of 12 ml/min of Ar, then pretO_2 (5 % O_2 in Ar, 13 ml/min total gas flow) was applied, and then pretH_2 (5 % H_2 in Ar, 12 ml/min total gas flow) before cooling to RT and flushing with Ar with 12 ml/min total gas flow (Figure 24).

3.6.2 CO adsorption and reaction conditions

After the pretreatment took place a CO adsorption experiment was performed. The sample was exposed to 2 ml/min of CO in Ar (12 ml/min total flow rate) until the IR band of CO stopped changing substantially. Next, 12 ml/min of Ar was circulated through the cell until there were no more changes in the IR spectra. After completing the CO adsorption experiment the catalyst was measured while undergoing the WGSR a gas mixture containing 5.55% CO (due to a limited gas flow controller) and 1.84% of H_2O in Ar (18 ml/min total gas flow) with the same heating scheme that is described in the catalytic activity studies (3.5.2). After the reaction finished, the system was flushed again with Ar and cooled to RT, the CO adsorption experiment was then repeated.

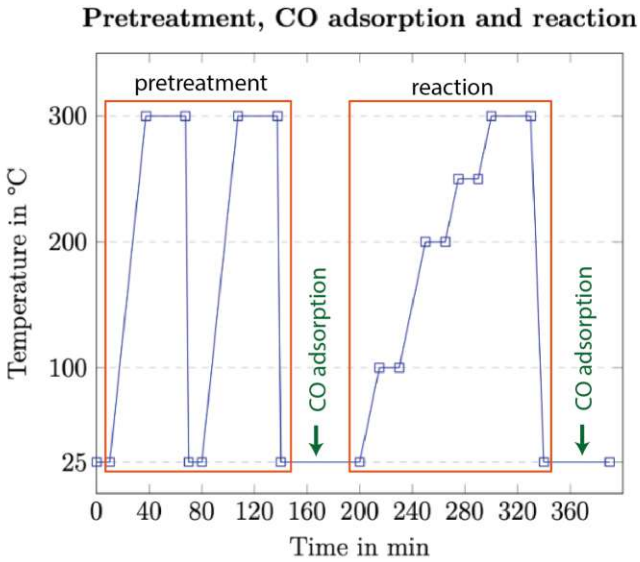

Figure 24: Heating scheme during pretreatment, CO oxidation experiment and during the WGSR for the operando IR DRIFT studies

4 Results and discussion

4.1 Kinetic tests

For every synthesised catalyst the results of the catalytic activity study are displayed in Figure 25, 26 and 27. The CO conversion rates at various temperatures can be seen in 25. It should be mentioned that the test also assessed the support itself as well, since it contributes to the catalytic activity to a small extent. Only at temperatures above 200

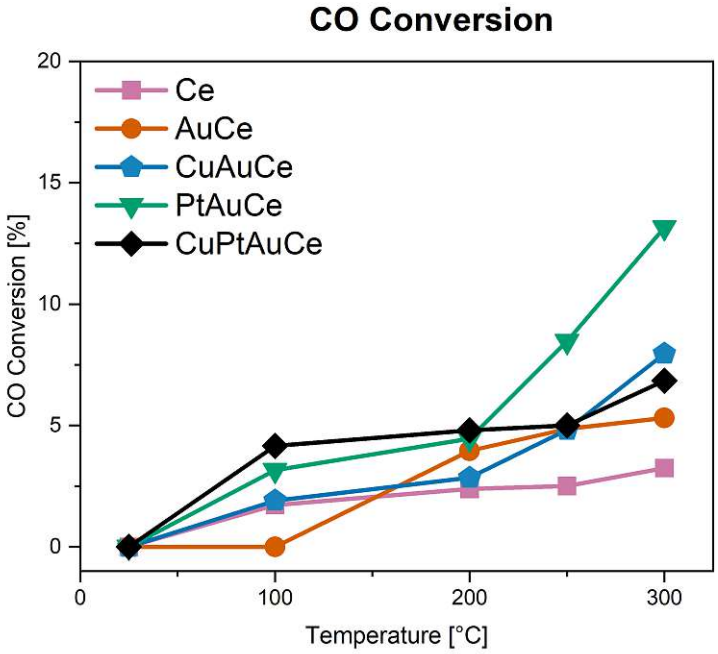

Figure 25: Results for the CO conversion of the kinetic tests for all catalysts.

°C is it possible to observe how the catalyst affects the catalytic performance, beyond 200°C it is possible to see the CO conversion rate increase the most. The maximum conversion rate was exhibited by PtAuCe, which was subsequently followed by CuAuCe, CuPtAuCe, and then AuCe. The CO conversion for PtAuCe is already relatively high at the beginning compared to the other catalysts and also increases the most, already at temperatures of 200°C. The other catalysts, however, show a higher CO conversion at a temperature of 250°C, with a flatter increase. Overall, among the catalysts examined for the WGSR, bimetallic catalysts showed the best performance and with the trimetallic catalyst following, the doping increased the catalytic activity overall. The creation of H_2 and CO_2 (Figures 26 and 27) demonstrates comparable results.

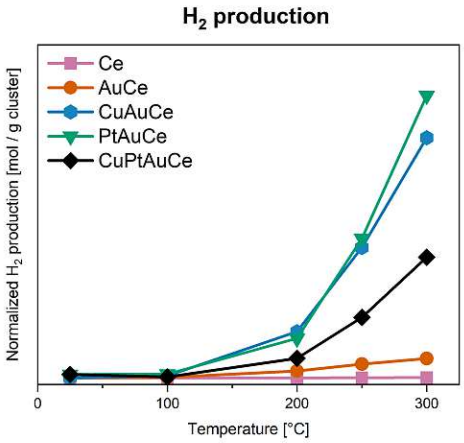

Figure 26: Results for the H_2 generation of the kinetic tests for all catalysts.

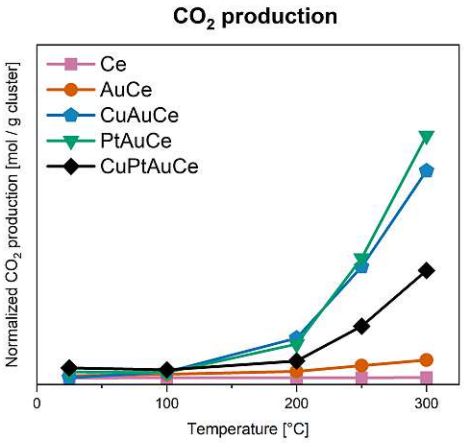

Figure 27: Results for the CO_2 generation of the kinetic tests for all catalysts.

Each catalyst produced both the products in roughly similar amounts, yielding a selectivity of 50% for each, which therefore results in a probability of 50% for the production of both products. Since each catalyst produced a different set of results, it is assumed, that the adsorption and catalysis processes would have to differ from each other since the experiments conditions remained the same throughout and results could be reproduced. As an example, the CuPtAuCe did not achieve better results than the bimetallic catalysts. Therefore, it is suspected, that the interaction of the doping atoms must be different, or maybe interfering with each other. With CuPtAuCe, a higher CO conversion can only be attained at a higher temperature. Compared to the other catalysts, CuPtAuCe initially showed promising CO conversions in the beginning at lower temperatures, but the overall increase in CO conversion has remained relatively low in comparison to the bimetallic catalysts, by which he is ultimately surpassed at 250°C. It might be possible to increase the temperature in future experiments to see if the catalytic activity increases then. It may therefore be necessary to conduct further research in order to identify the best catalyst for the reaction. Additionally, it may be necessary to optimize the catalyst used and the reaction conditions.

To assess the initial "stability" of the catalyst surface, the conducted measurement of the WGSR in the kinetic tests was repeated under the same conditions. The stability tests can be a helpful indicator of any surface structure changes that might affect the catalysts ability to adsorb the reactants during the WGSR, which then also effects CO conversion and product production. It is important to note that the focus here is on the possible structural changes of the catalysts after a reaction has taken place. The real stability of the catalyst would have to be tested with more repetitions. The stability test for the catalysts AuCe (Figure 28) and CuAuCe (Figure 28) resulted in a decrease of CO Conversion, H_2 and CO_2 production of approximately 1% each, which indicates that the surface should have remained consistent and therefore stable.

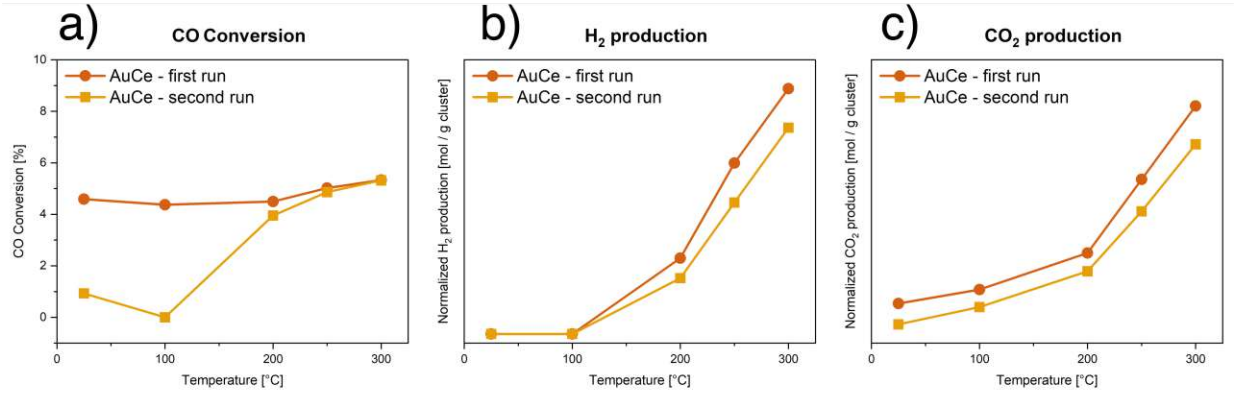

Figure 28: Kinetic test results of two consecutive kinetic test runs for the AuCe catalyst.

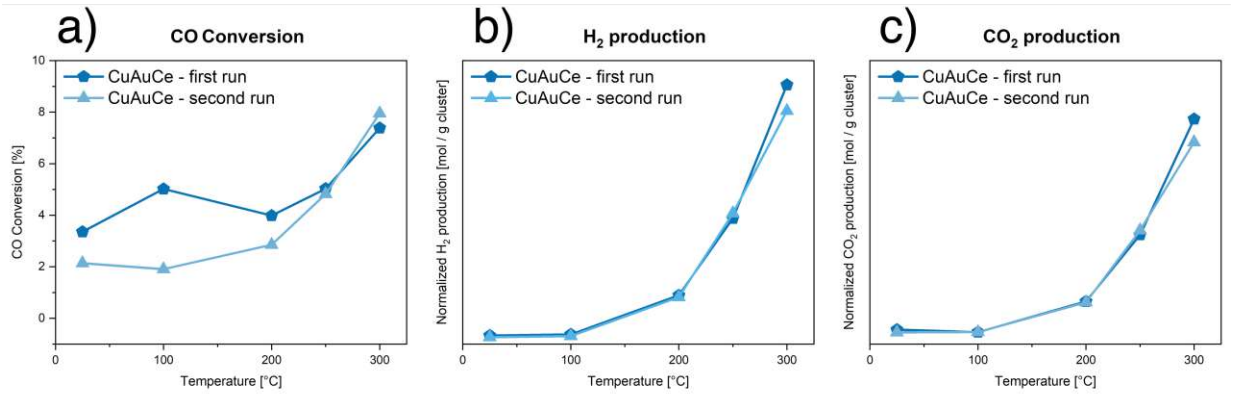

Figure 29: Kinetic test results of two consecutive kinetic test runs for the CuAuCe catalyst.

The stability test for the catalysts PtAuCe (Figure 30) resulted in a decrease of CO Conversion, H_2 and CO_2 production of approximately 1.5% each, which is also still considered stable.

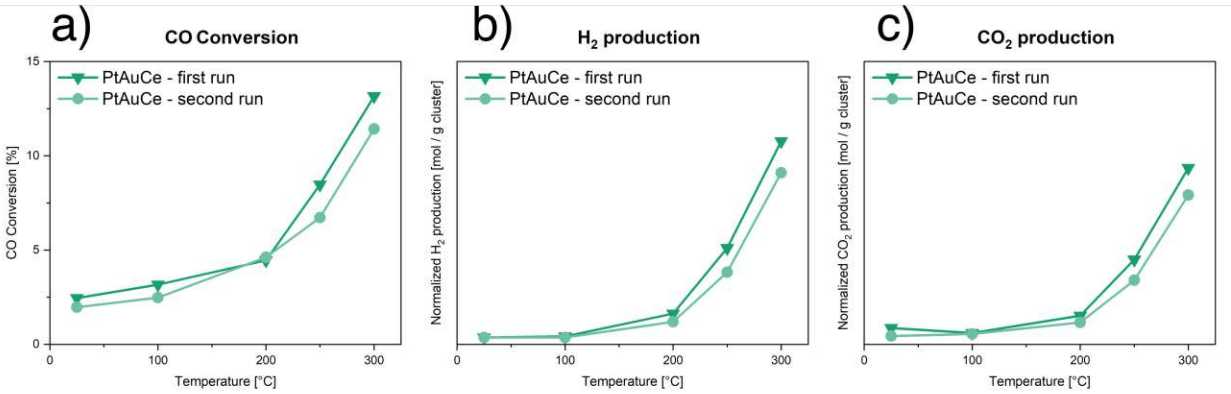

Figure 30: Kinetic test results of two consecutive kinetic test runs for the PtAuCe catalyst.

However, CuPtAuCe (Figure 31) exhibited in the stability test a decrease of CO Conversion of approximately 5% and a decrease in H_2 and CO_2 production of approximately 65%. The results indicate that the catalyst surface is not stable for two consecutive runs. Therefore, the catalyst structure was likely influenced and affected after it underwent the first reaction. It is assumed that the number of active sites, was ready reduced after the first reaction wich resulted in the decrease of CO conversion and product generation. It is

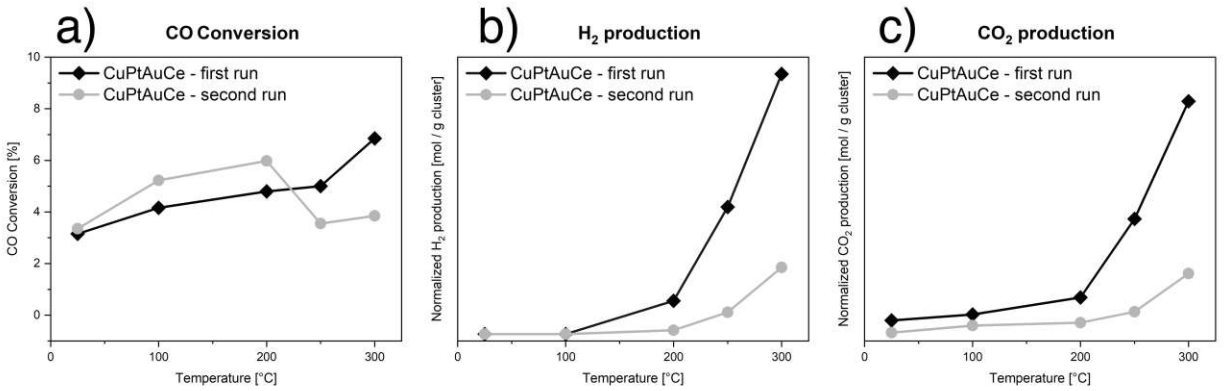

Figure 31: Kinetic test results of two consecutive kinetic test runs for the CuPtAuCe catalyst.

still necessary to conduct more research with more runs in order to fully understand catalyst stability over time. However, the current focus is determining how different dopant atoms affect catalytic activity, as their effects vary. Adsorption mechanisms for reactants and products are therefore further investigated, allowing us to determine how geometrical variations affect the catalysis as well as which atoms participate in the reaction and to what extend.

4.2 Operando IR DRIFTS

It is important to comprehend how the cluster structure impacts the reaction, to explain the variations in catalytic activity, which has been measured. The question of whether the variations in CO adsorption on the surface are caused by geometrical variations emerges, considering the different results for the catalytic activity. To determine the active sites of the catalysts, and, if CO is available for the reaction, CO adsorption experiments were carried out after the pretreatment and the reaction. The CO adsorption tests were repeated to check for any changes in the catalyst's surface after the WGSR. The spectrum of gas-phase CO falls within the range of 2250 - 2050 cm^{-1}, which may potentially overlap with bands from adsorbates.[62] Given the optical path length in the dead volume of the cell, this needs to be considered for DRIFT measurements. To correct for the presence of gas phase CO, a reference spectrum was obtained using a KBr matrix under identical reaction conditions, as KBr does not adsorb CO. However, it should also be mentioned that the assignment of the adsorption bands is not always straight forward, as there are always interactions and deviations due to various influences.[63] The CO-Au adsorption for

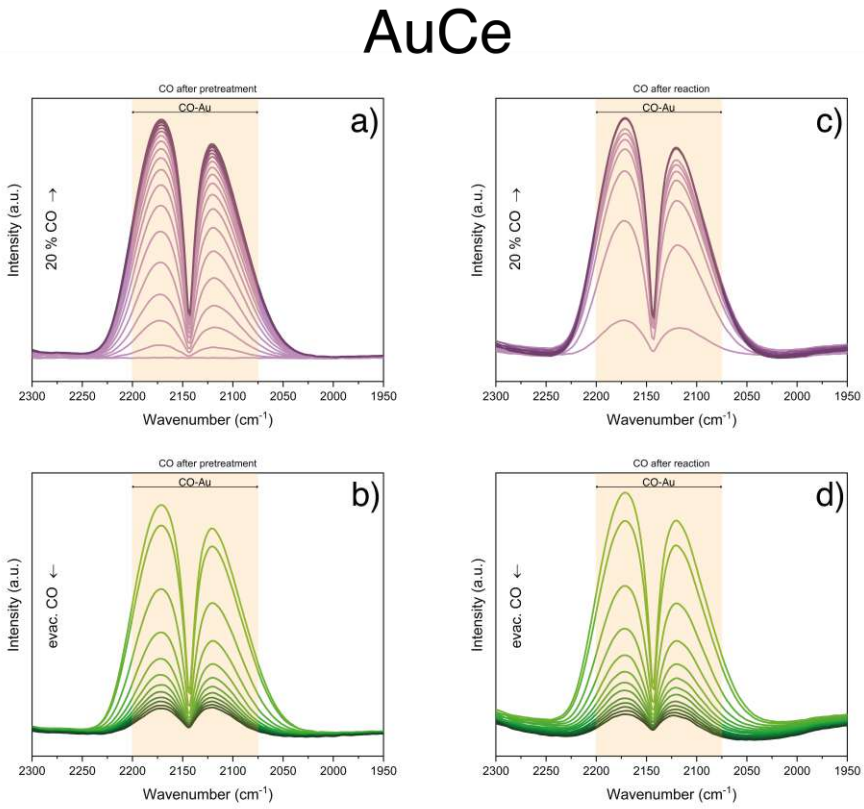

Figure 32: CO adsorption experiment of AuCe after the pretreatment a) and b) and after the reaction c) and d).

monometallic, neutral, and positively charged Au species (supported by various materials), ranges from 2075 to 2200 cm^{-1}, according to some studies.[63,64] The CO signal seen on the monometallic AuCe (Figure 32) has two maxima at 2175 and 2120 cm^{-1}. Despite being attributed to CO adsorbed on negatively charged Au clusters (2080–2000 cm^{-1}), it is assumed that this species does not exist since no peaks in this area are present. Bands below 2075 cm^{-1} are also an indication, that CeO_{2-x} oxygen vacancies are present, which is therefore probably not present in these samples. Here negatively charged Au particles accumulate up on CeO_{2-x} oxygen vacancies.[63] The second greatest peak at 2120 cm^{-1} would fall between the bands between 2120 and 2080 cm^{-1}, which are frequently linked to CO adsorbed at metallic gold edges or other defects (O-Au-CO). This peak can typically be seen on gold catalysts that are supported on ceria or titania after oxygen is incorporated with pre-adsorbed CO present. And indicates, that the Au-O sites are the result of an interaction between Au and oxygen from the substrate.[63] From above 2140 cm^{-1} the bands can be assigned to CO adsorbed on positively/cationic charged $Au^{\delta+}$ with low charges ($\delta < 1$) situated at lower wavenumbers and high charges situated at higher wavenumber. Therefore, the maximum peak at 2175 cm^{-1} is thought to be caused by Au^{III}, since the high wavenumber indicates a high oxidation state.[64] The peaks higher height suggests that there are more Au^{III} than O-Au-CO sites present. Although there could still be an overlap with other peaks, such as a peak at 2103 cm^{-1} would indicating CO adsorbed on metallic gold (CO-Au^0),[64] the results suggest that there are no Au^0 sites present in the AuCe catalyst. During the CO dosing experiment, it was observed that both maxima decreased while some residual CO remained on the surface even after flushing with inert gas. In the repeated CO-dosing experiment after the reaction on AuCe, no apparent changes were observed compared to the previous dosing experiment after pretreatment, suggesting that the CO-adsorption sites on the catalyst remained. A remaining binding site could indicate that CO becomes available already from the binding sites for the reaction. This is further supported by the stability test, which showed no concerning decrease in catalytic activity. The spectra also indicate that the binding site of Au^{III} is favoured to the O-Au-CO site due to the difference in intensity.

For CuAuCe (Figure 33) a signal was measured from 2050 to 2200 cm^{-1} with three broad maxima observed at 2165, 2112, and 2073 cm^{-1}. However, it is important to note, that the area for CO-Au bonding sites and CO-Cu bonding sites overlap. While the two maxima at 2165 and 2112 cm^{-1} could still be attributed to CO-Au binding sites of CO-Au^{III} and O-Au-CO sites like seen with AuCe (Figure 32), but a shift towards lower wavenumbers was also noticed which could be due to the Cu doping. The change to a lower wavenumbers and peak at 2073 cm^{-1} indicates that the Cu adsorption sites are electron deficient. Typical wavenumbers for CO-Cu^0 sites are below 2100 cm^{-1} which agrees with the received spectrum. When directly in contact, copper atoms might become electron deficient due to the high electronegativity of gold. Of course, CuAu alloys are susceptible to this process. It is therefore possible for an electron to pass from Cu to Au, which causes a deficiency of electrons in the Cu atoms.

The higher intensity peak at 2112 cm^{-1} is therefore also hard to assign. It could still be

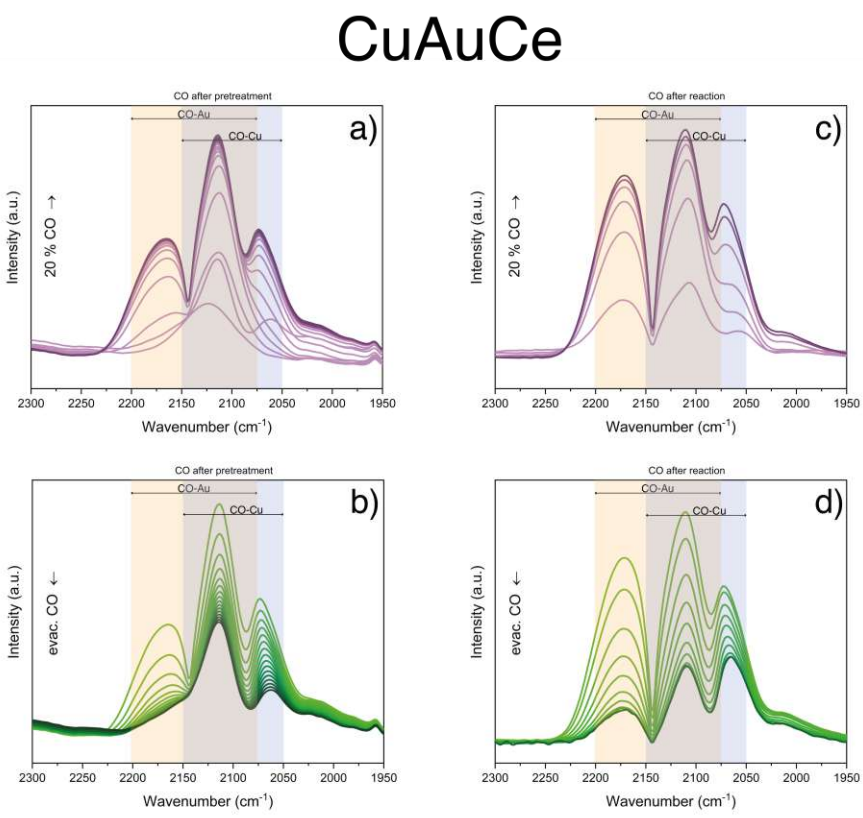

Figure 33: CO adsorption experiment of CuAuCe after the pretreatment a) and b) and after the reaction c) and d).

attributed to O-Au-CO species like with AuCe, due to the shift to lower wavenumbers. A peak, which was then also previously measured by other researchers at 2125 cm^{-1} can be

assigned to Au-Cu^+.[63,64] Another possibility is, that the intensity could be attributed to CO-Cu^I sites, which typically adsorb at around 2120 cm^{-1}. It is therefore very likely that several bonding sites overlap here, which also leads to the higher intensity. As a result, the increase in catalytic activity could be due to the creation of more possible bonding sites for either O-Au-CO, Au-Cu^+, CO-Cu^I, or a mixture of all three. It is possible that the increase in catalytic activity, compared to AuCe, resulted from an increase in the number of active sites for CO bonding, as a direct result of the Cu doping.[63,64] In addition, according to other research, CO adsorption on Cu^{2+} sites is generally not observed.[63] The broad maxima at 2165 cm^{-1} can then be ascribed to Au^{III}-CO bonding sites. Throughout the CO adsorption experiment the adsorption sites of the CO remains the same, but the dosing after the reaction showed different intensities. The intensity for the adsorption site at 2165, and 2073 cm^{-1} increased while the one at 2112 cm^{-1} decreased. Since approximately the same CO conversion was measured, it may be assumed that by creating the adsorption site at 2165 cm^{-1} and increasing it at 2073 cm^{-1} in regards of CO staying available for the reaction, the number of active sites balances out and thus the catalytic activity is less affected.

For PtAuCe (Figure 34 a signal between 2000 to 2200 cm^{-1} with again three maxima at 2175 and 2112 and 2045 cm^{-1} could be obtained. Based on previously performed other studies regarding Pt/CeO_2 and CO adsorption on Pt, at around 2000 to 2040 cm^{-1} the adsorption of CO on Pt single atoms in cluster is normally observed.[62] If the Pt atom is positively charged however, the adsorption of CO will take place at higher wavenumbers. This means that CO-Pt adsorption sites could be overlapping with CO-Au adsorption sites. Between 2040 - 2070 cm^{-1} CO can adsorb on positively charged Pt^{2+}, creating CO-Pt^{2+} sites. At around 2090 - 2125 cm^{-1} CO-Pt^{4+} binding sites have been reported.[62]

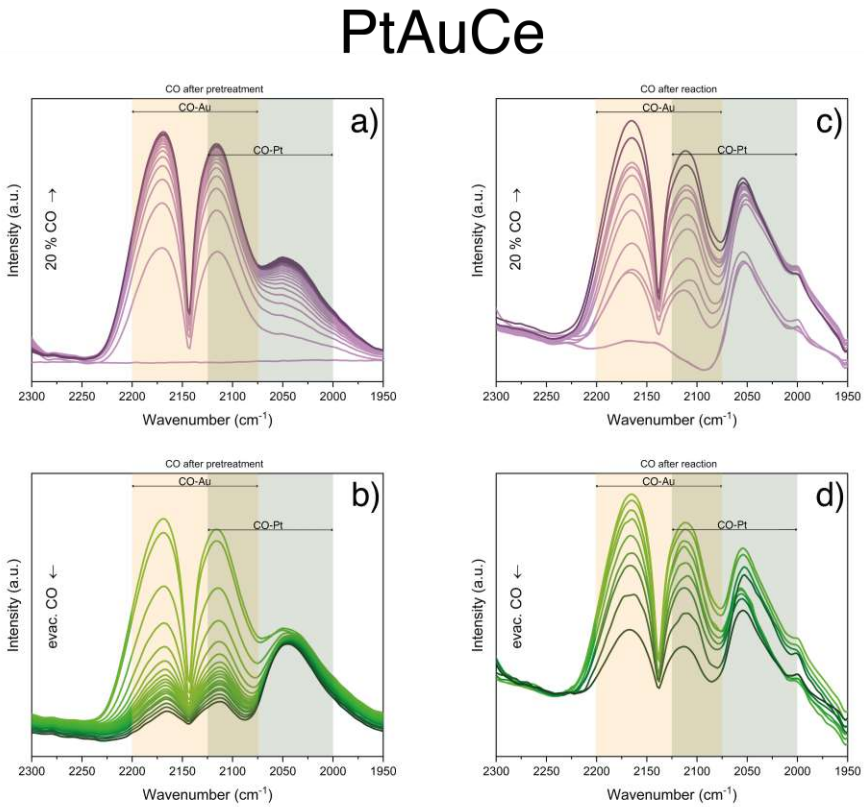

Figure 34: CO adsorption experiment of PtAuCe after the pretreatment a) and b) and after the reaction c) and d).

Although, most of the spectrum is affected by possible overlapping the maxima at 2175 cm^{-1} is attributed to CO-Au^{III} bonding sites, since at this area only CO-Au bonding can be possible for this type of PtAu alloy, due to other reports.[62,63] The broad peak observed at 2045 cm^{-1} is more likely to be CO-Pt^0, but it could also be CO-Pt^{1+} since this peak can be observed starting at 2040 cm^{-1}. However, due to the broadness of the peak, it is more likely that CO-Pt^0 is the dominant species present, since positively charged Pt binding sites should have a higher wavenumber for CO-Pt adsorption. The peak at 2112 cm^{-1} could still be attributed to O-Au-CO bonding sites, but the area and increased intensity may be due to overlapping with CO bonding to positively charged Pt species, most likely Pt^{4+}. Due to the two maxima with a lower wavenumber "merging" together with more CO gas being adsorbed, a Pt^{2+} bonding site, which can lie in between, cannot be excluded as a possible binding site.[62] Overall, the intensities for all adsorption sites for CO increase significantly. CO remains left behind on the catalyst surface, even after flushing with inert gas. Therefore, it is possible that CO might be available for the reaction. The intensity of the remaining CO species after the reaction also shows no

significant changes between the different CO-dosing experiments, which could explain the consistent CO conversion and product gas generation. In general, a lot of CO adsorption could be observed in the spectrum here, which could be the reason for the good catalytic activity of PtAuCe. It is also apparent that the processes involved in CO adsorption are different from those detected in the case of AuCe and CuAuCe studied so far due to different adsorption mechanisms, although certain binding sites, most likely from CO-Au, may have remained the same.

After analysing the measured spectra, it was surprising to find that CuPtAuCe did not exhibit the previously observed characteristic peaks for CO-Cu and CO-Pt. In the case of CuPtAuCe (Figure 35), a signal between 2050 to 2200 cm^{-1} was obtained with only two maxima at 2175 and 2125 cm^{-1}. However, unlike the other catalysts, no third maximum could be observed here that could normally be attributed to CO-Cu and CO-Pt peaks. Only when evacuation with inert gas was performed, a small "shoulder" peak was observed at around 2065 cm^{-1}. The two maxima are more likely due to CO-Au bonding sites of CO-Au^{III} (maximum at higher wavenumber) and O-Au-CO (maximum at lower wavenumbers) on the catalyst surface. It was also observed that CO dosing before and after the reaction was significantly different. After the first dosing experiment, CO was remaining on the catalyst surface after flushing with inert gas, but this was not the case when CO dosing was repeated after the reaction. Then, almost no CO bonding was observed on the previously possible sites of CO-Au^{III} and O-Au-CO. Only a small amount of remaining CO adsorbed around 2065 cm^{-1}. It is likely that there are no or only a low number of possible Cu-CO or Pt-CO binding sites that still could be ascribed to this small peak. This could explain the reduction in CO conversion and product gas generation during the repeated kinetics tests with the trimetallic catalyst. It is suspected that the doping with Cu and Pt may be blocking possible surface sites on the catalyst and hinder CO adsorption, rather than increasing the amount of possible CO adsorption. This may explain the relatively low catalytic activity of the catalyst compared to the bimetallic ones.

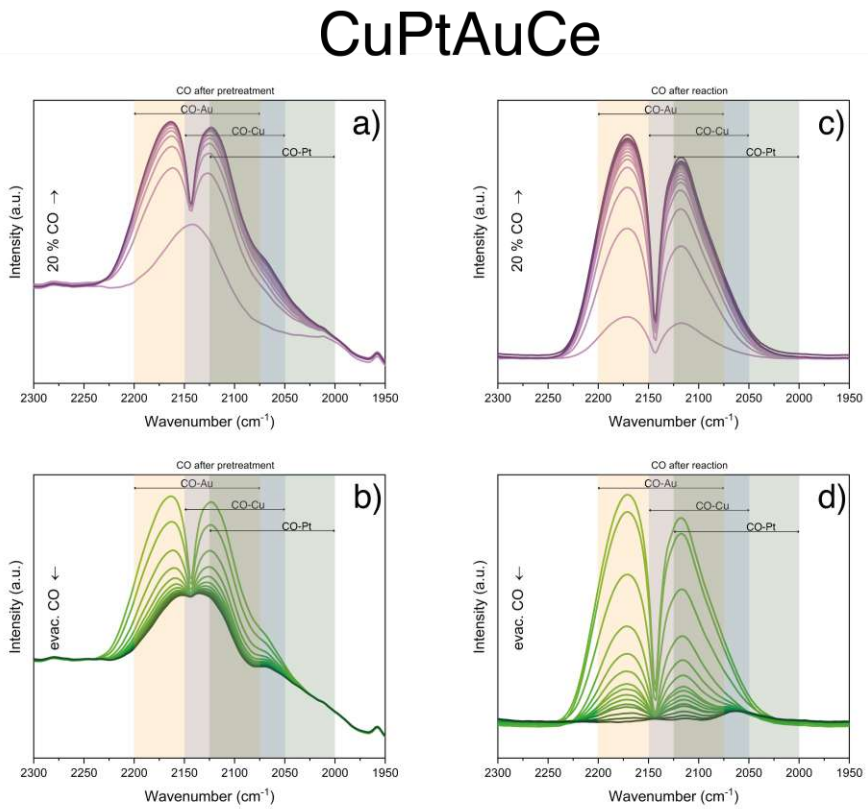

Figure 35: CO adsorption experiment of CuPtAuCe after the pretreatment a) and b) and after the reaction c) and d).

The other spectral areas H_2O-bonding and C-bonding can be seen in the Appendix. The progress of the reaction can be monitored in the area between 1900 and 2500 cm^{-1}, where CO and CO_2 are adsorbed (Figure 38).[64]

At 2340 cm^{-1}, physiosorbed CO_2 can be observed. If CO_2 is detected already at lower temperatures or even RT, that the detection of CO_2 present is most likely due to the reaction between already-adsorbed CO and lattice oxygen. This occurrence can not only be seen in the IR DRIFT spectra of all the prepared catalyst but could also be detected during the kinetic tests of AuCe, PtAuCe, and CuPtAuCe. It can therefore be assumed that the interaction between adsorbed CO and lattice oxygen can produces CO_2, while the lack of CO_2 at lower temperatures can imply that continuously supplied oxygen is missing and that the oxygen is not activated.[64] Yet, the presence of CO_2 adsorbed is still a good indication that the reaction is still ongoing, especially when the intensity is changing. It's interesting to note that in the case of CuAuCe and PtAuCe, at higher temperatures, less CO is bonded, which is likely due to it being used in the reaction. This behaviour is not

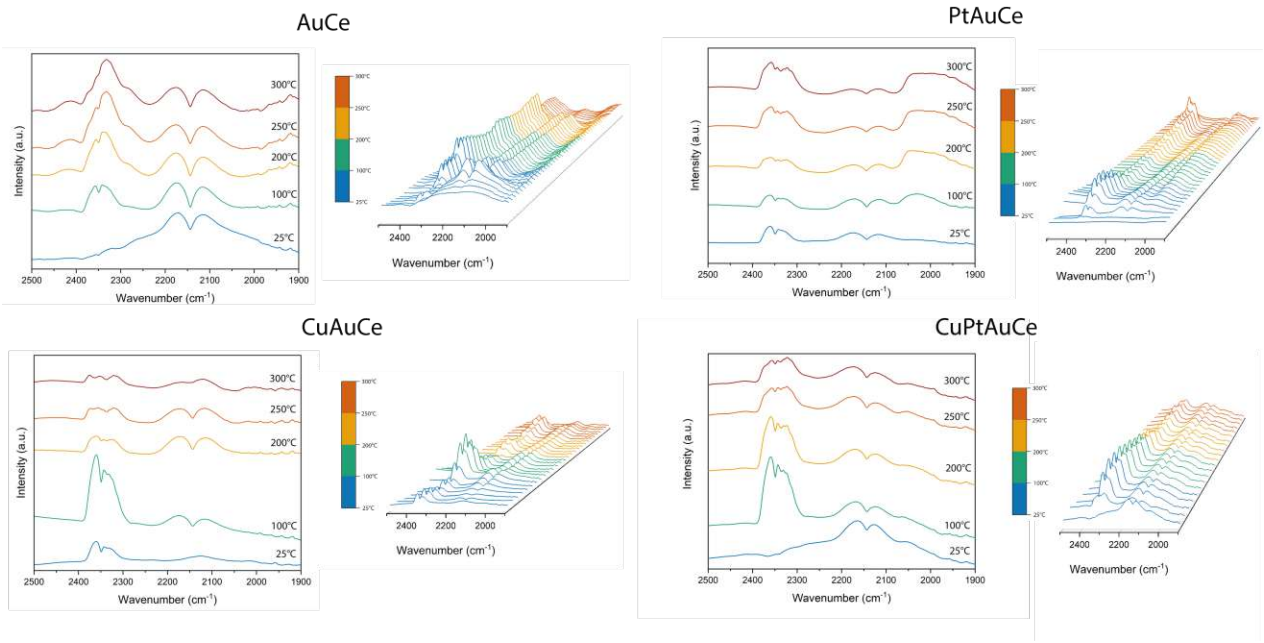

Figure 36: Operando IR DRIFT spectra of the prepared catalysts as the reaction progresses.

observed in AuCe and CuPtAuCe, which showed the least catalytic activity, where the amount of CO adsorbed roughly stays the same or even increases. Also noticeable, is, that during the reaction, the binding site between CO-Pt keeps CO adsorbed, even at high temperatures. However, it's not entirely clear whether this bound CO is also available for the reaction. Overall, these observations suggest that the behavior of CO on different catalysts is closely related to their catalytic activity. More experiments in this direction are needed to clarify which CO binding sites are more involved during the reaction to really understand how they affect the catalysis. However, a further investigation in total is necessary to determine the underlying mechanisms and optimize these catalysts for maximum efficiency.

4.3 Correlation to XANES and EXAFS studies

In situ measurements at the Au L_3-edge and Cu K-edge in fluorescence mode under reaction conditions in a flow cell reactor (CLAES beamline, ALBA) with the same conditions as in the IR DRIFT studies were conducted by the group previously and preliminary results could already be evaluated. X-ray absorption fine structure spectroscopy (XAFS) operando on the Au L_3-edge and Cu K-edge examined the possible dynamic structure of supported nanoclusters in regard to pretreatments, reaction conditions and stability in regard to their doping type.

4.4 Cu K-edge

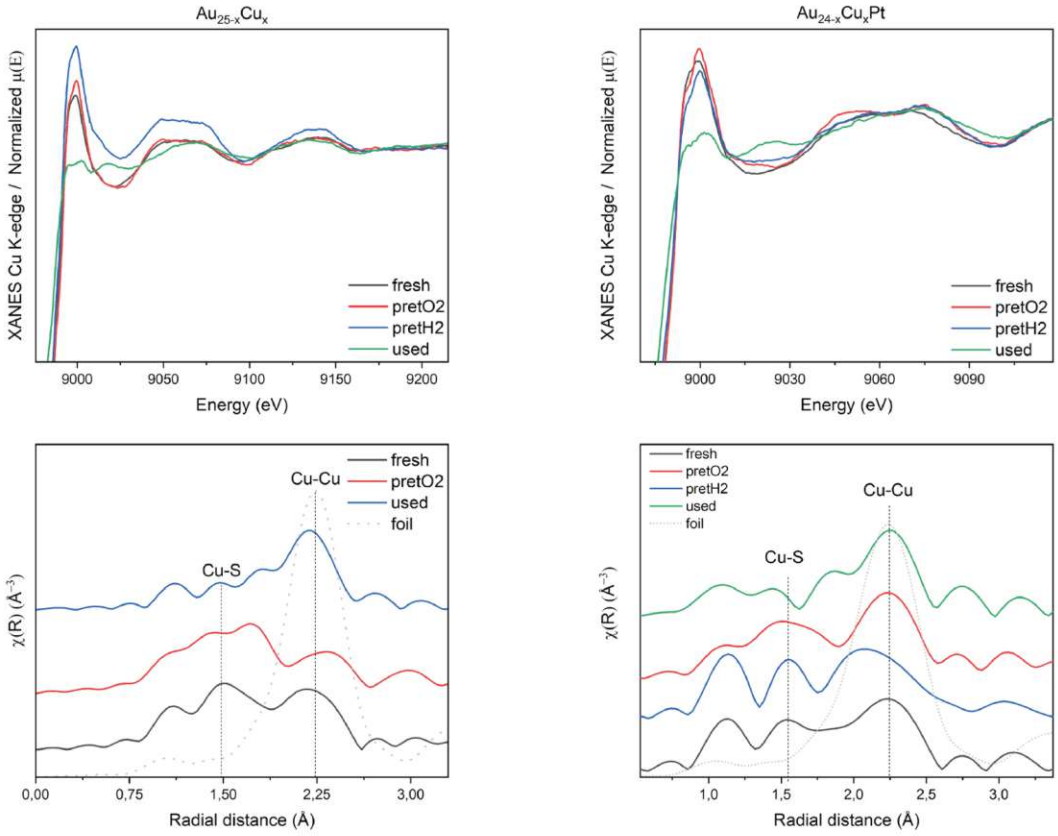

Figure 37: Cu K-edge with the results of the XANES and EXAFS of the bimetallic clusters.

Based on the results of the experiment (Figure 38, it was observed that Cu was partially charged which could be an indicator of $Au - Cu^{+}$ species in correlation with the IR DRIFT measurements. On the other hand, the EXAFS experiment revealed the visibility of Cu-Cu bonding, suggesting the formation of Cu "islands". The Cu islands could be

crucial for the CO bonding, since it could provide new adsorption sites for CO in form of metallic copper. It is yet unclear which contributes more for the catalytic activity.

4.5 Au L_3-edge

For the Pt-Au species, the XANES experiment showed that the Au-S bond was visible before the experiment, which is due to the cluster structure with thiol staples. However, after pretreatment, the Au-Metal bond (Au-Pt) became visible. This observation indicates that the pretreatment process led to the formation of stable Au-Pt clusters, which remained intact during the experiment. Overall, the XANES experiment suggests that the pretreatment plays a crucial role in the formation and stability of metal clusters. This is crucial for the catalytic activity, since the Pt dopant atoms serves as a binding site for CO adsorption. This could also be confirmed by the IR DRIFT studies, since CO bonded on the right region for CO-Pt adsorption sites and for the PtAuCe catalyst an increased catalytic activity could be measured.

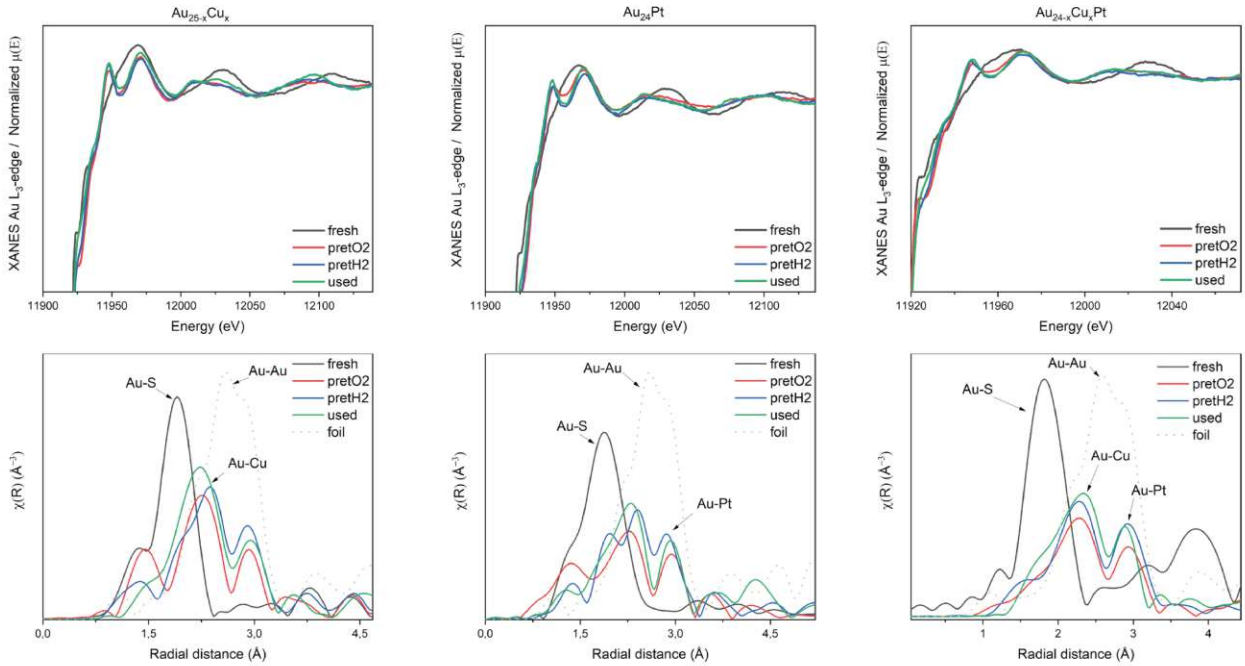

Figure 38: Au L_3-edge with the results of the XANES and EXAFS of the bimetallic and trimetallic clusters.

5 Conclusion

In conclusion, the catalytic activity of nanoclusters in the WGSR and the impact of their doping atoms was investigated. The results demonstrate, that the catalytic activity was enhanced by the inclusion of metal nanoclusters, and the bimetallic nanoclusters, especially the Pt doped PtAuCe, showed the greatest yield with about 50% selectivity to each desired product. In addition, the bimetallic clusters surface remained stable regarding CO conversion and product gas production after two consecutive runs. It has also been determined that the influence of the dopant atoms differs. Therefore, different adsorption processes for Cu and Pt doped catalysts must exist. With the Pt doped catalyst we can see, that the migration of the Pt doping atom leads to the creation of new bonding sites for CO adsorption and therefore an increased catalytic activity. For the Cu doped CuAuCe catalyst, the formation of Cu "islands" and partially charged Cu species was observed, which also results in the increase of binding sites of CO and a better catalytic activity. However, CuPtAuCe showed a reduced catalytic activity and stability. This means that the positive effects caused by both doping atoms Cu and Pt could not be combined, at least for now. It is assumed that the dopant atoms somehow interfere with each other and thus the surface of the catalyst changes, resulting in another surface adsorption process for CO during the reaction. It can also be, that the dopant atoms are blocking each others binding sites for CO, resulting in the decrease of catalytic activity. The operando IR DRIFTS revealed that the CO bond on the catalyst surface is significantly influenced by the nature of the active sites, which are dependent on the doping atom, since the CO adsorption resulted in different IR spectra. Overall, the results offer insightful understandings into the complex interaction between catalyst geometry and catalytic activity. For future investigation purposes, bimetallic NC catalysts could be researched for other reactions, and a further investigation of trimetallic doped system should be carried out to determine if the cluster could still be adjusted to meet the needs of the reaction for an improvement of the catalytic activity. Of course, the bimetallic cluster can be further adjusted with different doping atoms, cluster structures, and supports in future research. These catalysts offer great potential due to the promising results that have been observed.

Appendices

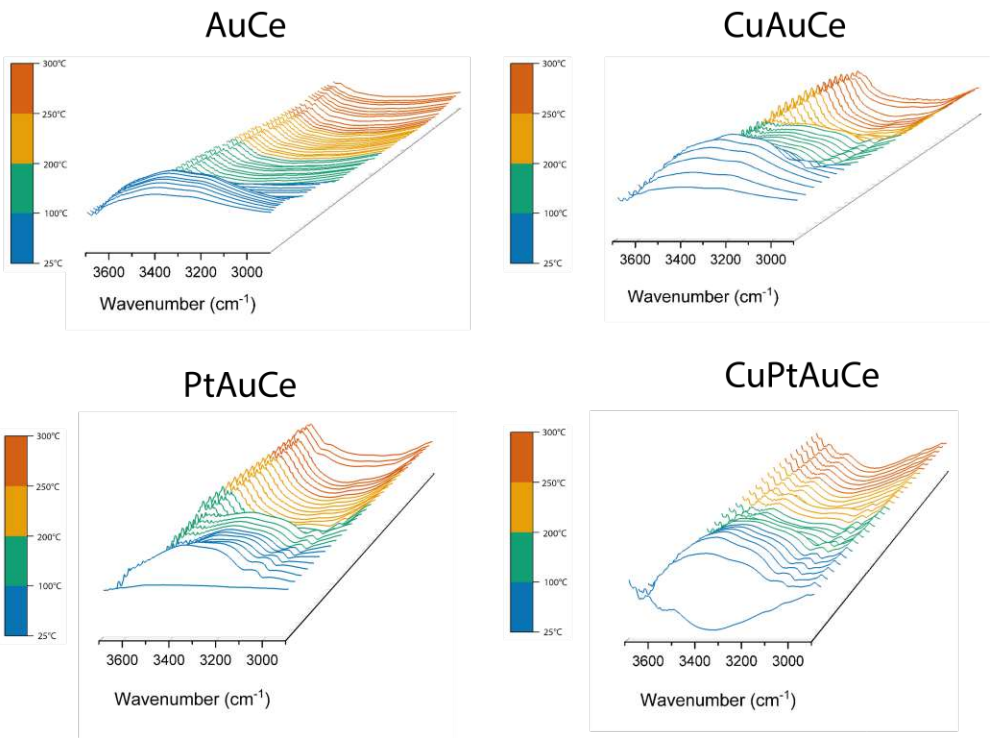

Figure A1: Operando IR DRIFT spectra of the prepared catalysts as the reaction progresses, H_2O-bonding area.

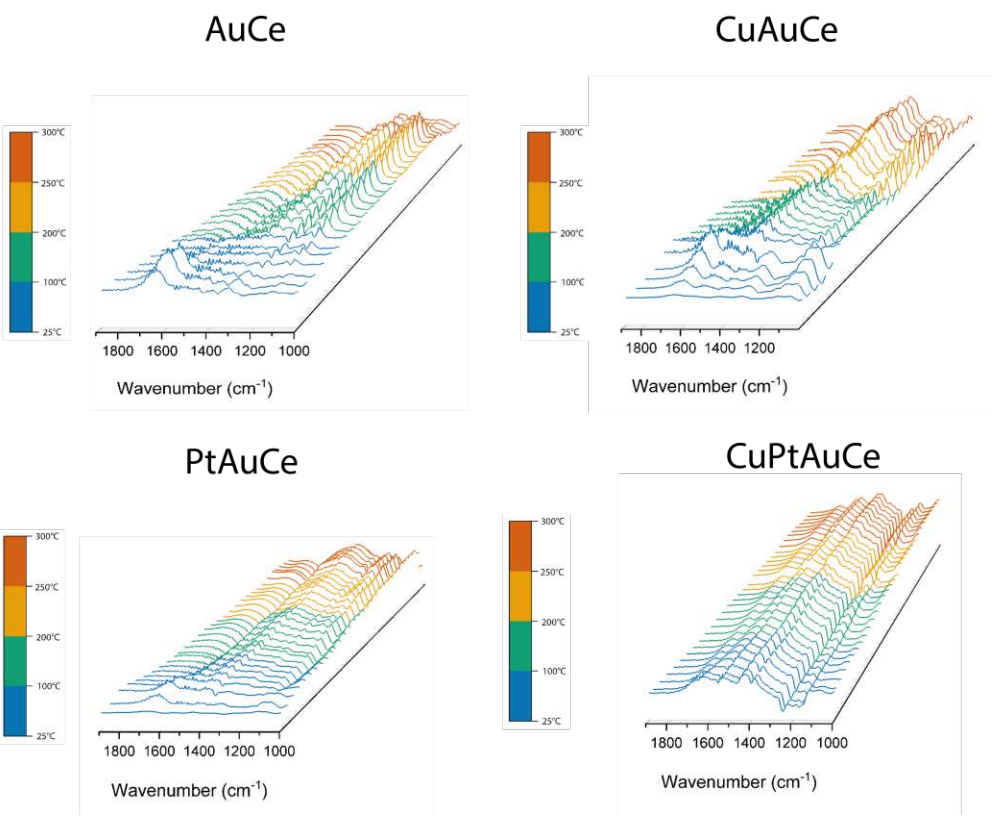

Figure A2: Operando IR DRIFT spectra of the prepared catalysts as the reaction progresses, C-bonding area.

Table A1: List of used chemicals

Chemical formula	**Name**	**Abbrev.**	**CAS No.**	**Purity**	**Suplier**
C_4H_8O	Tetrahydrofuran	THF	109-99-9	inhibitor-free, suitable for HPLC, 99.9%	Sigma-Aldrich
$C_{32}H_{68}BrN$	Tetraoctylammonium bromide	TOAB	14866-33-2	>98.0%(T)	TCI Germany
$C_6H_5CH_2CH_2SH$	2-Phenyl-ethanthiol	2-PET	4410-99-5	99%, FG	Sigma-Aldrich
$NaBH_4$	Sodium borohydrid	x	16940-66-2	purum p.a., 96% (gas-volumetric)	Sigma-Aldrich
CH_3OH	Methanol	MeOH	67-56-1	ROTISOLV® HPLC Gradient Grade	Carl Roth
CH_2Cl_2	Dichloromethane	DCM	75-09-2	ROTISOLV® HPLC	Carl Roth
$HAuCl_4 \cdot 3\,H_2O$	Tetrachlorogold(III)-acid Trihydrat	x	16961-25-4	99,9 %, p.a., Ultra Qualität	Carl Roth
C_2H_3N	Acetonitrile	x	75-05-8	OmniSolv® LC-MS	Sigma-Aldrich
C_3H_6O	Aceton	x	67-64-1	HPLC Plus, for HPLC, GC, and residue analysis, 99.9%	Sigma-Aldrich
C_2H_3N	Acetonitrile	x	75-05-8	OmniSolv® LC-MS	Sigma-Aldrich
$CuCl_2 \cdot 2\,H_2O$	Copper (II) Chloride	x	10125-13-0	ACS reagent, 99.0%	Sigma-Aldrich
$C_2H_8N_2$	Ethylenediamine	EDA	107-15-3	puriss. p.a., absolute, 99.5% (GC)	Sigma-Aldrich
C_2H_6O	Ethanol	EtOH	64-17-5	ROTISOLV® HPLC Gradient Grade	Carl Roth
C_7H_8	Toluene	x	108-88-3	99.5%, for synthesis	Carl Roth
$C_8H_8O_4$	2,4,6-Trihydroxyacetophenon	x	480-66-0	98%	Sigma-Aldrich
CeO_2	Cer(IV)-oxid	x	1306-38-3	REacton®, 99.9% (REO)	Alfa Aesar
$(C_2H_4O)_n$	poly(vinyl alcohol)	x	9002-89-5	EMPROVE® ESSENTIAL, Ph. Eur., ChP, JPE, USP	Sigma-Aldrich

References

[1] S. R. Wan Alwi, J. J. Klemeš, and P. S. Varbanov, "Cleaner energy planning, management and technologies: Perspectives of supply-demand side and end-of-pipe management," *Journal of Cleaner Production*, vol. 136, pp. 1–13, 11 2016.

[2] N. Armaroli and V. Balzani, "The Future of Energy Supply: Challenges and Opportunities," *Angewandte Chemie International Edition*, vol. 46, no. 1-2, pp. 52–66, 2007.

[3] G. Cai, Y. He, H. Ren, Y. Zhan, C. Chen, Y. Luo, and L. Jiang, "Hydrogen production via water-gas shift reaction by Cu/SiO2catalyst: A case study of CeO2doping," *Energy and Fuels*, vol. 35, pp. 3521–3528, 2 2021.

[4] B. Smith R. J., M. Loganathan, and M. S. Shantha, "A review of the water gas shift reaction kinetics," *International Journal of Chemical Reactor Engineering*, vol. 8, 2010.

[5] L. L. Hegedus, "12 Catalyst Design," in *Advances in Chemical Engineering* (C. K. Colton, ed.), vol. 16, pp. 237–252, Academic Press, 1991.

[6] C. Gadipelly and L. K. Mannepalli, "Nano-metal oxides for organic transformations," *Current Opinion in Green and Sustainable Chemistry*, vol. 15, pp. 20–26, 2 2019.

[7] S. Pollitt, V. Truttmann, T. Haunold, C. Garcia, W. Olszewski, J. Llorca, N. Barrabés, and G. Rupprechter, "The Dynamic Structure of Au38(SR)24Nanoclusters Supported on CeO2upon Pretreatment and CO Oxidation," *ACS Catalysis*, vol. 10, pp. 6144–6148, 6 2020.

[8] J. Fang, B. Zhang, Q. Yao, Y. Yang, J. Xie, and N. Yan, "Recent advances in the synthesis and catalytic applications of ligand-protected, atomically precise metal nanoclusters," *Coordination Chemistry Reviews*, vol. 322, pp. 1–29, 9 2016.

[9] A. Aparna, H. Sreehari, A. Chandran, K. P. Anjali, A. M. Alex, P. Anuvinda, G. B. Gouthami, N. P. Pillai, N. Parvathy, S. Sadanandan, and A. Saritha, "Ligand-protected nanoclusters and their role in agriculture, sensing and allied applications," *Talanta*, vol. 239, p. 123134, 3 2022.

[10] N. Barrabés, J. Ostolaza, S. Reindl, M. Mähr, F. Schrenk, H. Drexler, C. Rameshan, W. Olszewski, and G. Rupprechter, "Doped metal clusters as bimetallic AuCo nanocatalysts: insights into structural dynamics and correlation with catalytic activity by in situ spectroscopy," *Faraday Discussions*, vol. 242, pp. 94–105, 1 2023.

[11] K. Yuan, X. C. Sun, H. J. Yin, L. Zhou, H. C. Liu, C. H. Yan, and Y. W. Zhang, "Boosting the water gas shift reaction on Pt/CeO2-based nanocatalysts by compositional modification: Support doping versus bimetallic alloying," *Journal of Energy Chemistry*, vol. 67, pp. 241–249, 4 2022.

[12] C. Garcia, V. Truttmann, I. Lopez, T. Haunold, C. Marini, C. Rameshan, E. Pittenauer, P. Kregsamer, K. Dobrezberger, M. Stöger-Pollach, N. Barrabés, and G. Rupprechter, "Dynamics of Pd Dopant Atoms inside Au Nanoclusters during Catalytic CO Oxidation," *Journal of Physical Chemistry C*, vol. 124, pp. 23626–23636, 10 2020.

[13] C. Zeng and R. Jin, "Chiral Gold Nanoclusters: Atomic Level Origins of Chirality," *Chemistry – An Asian Journal*, vol. 12, pp. 1839–1850, 8 2017.

[14] Y. Wang and T. Bürgi, "Ligand exchange reactions on thiolate-protected gold nanoclusters," *Nanoscale Advances*, vol. 3, pp. 2710–2727, 5 2021.

[15] J. B. Park, J. Graciani, J. Evans, D. Stacchiola, S. D. Senanayake, L. Barrio, P. Liu, J. F. Sanz, J. Hrbek, and J. A. Rodriguez, "Gold, copper, and platinum nanoparticles dispersed on CeO(x)/TiO(2)(110) surfaces: high water-gas shift activity and the nature of the mixed-metal oxide at the nanometer level," *Journal of the American Chemical Society*, vol. 132, pp. 356–363, 1 2010.

[16] V. Palma, C. Ruocco, M. Cortese, S. Renda, E. Meloni, G. Festa, and M. Martino, "Platinum Based Catalysts in the Water Gas Shift Reaction: Recent Advances," *Metals 2020, Vol. 10, Page 866*, vol. 10, p. 866, 6 2020.

[17] N. L. Wieder, M. Cargnello, K. Bakhmutsky, T. Montini, P. Fornasiero, and R. J. Gorte, "Study of the water-gas-shift reaction on Pd@CeO2/Al 2O3 core-shell catalysts," *Journal of Physical Chemistry C*, vol. 115, pp. 915–919, 2 2011.

[18] A. Sandoval, A. Gómez-Cortés, R. Zanella, G. Díaz, and J. M. Saniger, "Gold nanoparticles: Support effects for the WGS reaction," *Journal of Molecular Catalysis A: Chemical*, vol. 278, pp. 200–208, 12 2007.

[19] W. Z. Yu, W. W. Wang, C. Ma, S. Q. Li, K. Wu, J. Z. Zhu, H. R. Zhao, C. H. Yan, and C. J. Jia, "Very high loading oxidized copper supported on ceria to catalyze the water-gas shift reaction," *Journal of Catalysis*, vol. 402, pp. 83–93, 10 2021.

[20] X. Kang, H. Chong, and M. Zhu, "Au25(SR)18: the captain of the great nanocluster ship," *Nanoscale*, vol. 10, pp. 10758–10834, 6 2018.

[21] G. Li and R. Jin, "Atomically precise gold nanoclusters as new model catalysts," *Accounts of Chemical Research*, vol. 46, pp. 1749–1758, 8 2013.

[22] S. Hossain, Y. Imai, D. Suzuki, W. Choi, Z. Chen, T. Suzuki, M. Yoshioka, T. Kawawaki, D. Lee, and Y. Negishi, "Elucidating ligand effects in thiolate-protected metal clusters using Au24Pt(TBBT)18 as a model cluster," *Nanoscale*, vol. 11, pp. 22089–22098, 11 2019.

[23] R. Jin, "Quantum sized, thiolate-protected gold nanoclusters," *Nanoscale*, vol. 2, pp. 343–362, 3 2010.

[24] K. E. Lee, A. Shivhare, Y. Hu, and R. W. Scott, "Supported bimetallic AuPd clusters using activated Au25 clusters," *Catalysis Today*, vol. 280, pp. 259–265, 2 2017.

[25] S. Yamazoe, W. Kurashige, K. Nobusada, Y. Negishi, and T. Tsukuda, "Preferential location of coinage metal dopants (M = Ag or Cu) in [Au25- xMx(SC2H4Ph)18]- (x 1) as determined by extended X-ray absorption fine structure and density functional theory calculations," *Journal of Physical Chemistry C*, vol. 118, pp. 25284–25290, 10 2014.

[26] T. R. Reina, M. Gonzalez-Castaño, V. Lopez-Flores, L. M. Martínez T, A. Zitolo, S. Ivanova, W. Xu, M. A. Centeno, J. A. Rodriguez, and J. A. Odriozola, "Au and Pt Remain Unoxidized on a CeO2-Based Catalyst during the Water-Gas Shift Reaction," *Journal of the American Chemical Society*, vol. 144, pp. 446–453, 1 2022.

[27] A. M. Abdel-Mageed, G. Kučerova, J. Bansmann, and R. J. Behm, "Active Au species during the low-temperature water gas shift reaction on Au/CeO2: A time-resolved operando XAS and DRIFTS study," *ACS Catalysis*, vol. 7, pp. 6471–6484, 10 2017.

[28] E. Baraj, K. Ciahotný, and T. Hlinčík, "The water gas shift reaction: Catalysts and reaction mechanism," *Fuel*, vol. 288, p. 119817, 3 2021.

[29] A. A. Zagorodni, "Subjects that do not Fit in Other Chapters," *Ion Exchange Materials*, pp. 377–395, 1 2007.

[30] L. Arnaut and S. Formosinho, "Understanding Chemical Reactivity: The Case for Atom, Proton and Methyl Transfers," *Chemistry – A European Journal*, vol. 14, no. 22, pp. 6578–6587, 2008.

[31] F. Zaera, "Molecular approaches to heterogeneous catalysis," *Coordination Chemistry Reviews*, vol. 448, p. 214179, 2021.

[32] L. Poshyvailo, *Modelling and simulations of enzyme-catalyzed reactions*. PhD thesis, Forschungszentrum Jülich, National University of "Kyiv-Mohyla Academy" Faculty of Natural Sciences, Kyiv, 2015.

[33] S. T. Oyama1 and G. A. Somorjai, "Homogeneous, Heterogeneous, and Enzymatic Catalysis," *Journal of Chemical Education*, vol. 65, no. 9, pp. 765–769, 1988.

[34] R. Rangasamy, K. Lakshmi, and K. Muthu, "Chapter 15 - Sustainable catalysis of nanocrystals: A green technology," in *Industrial Applications of Nanocrystals* (S. Mallakpour and C. M. Hussain, eds.), pp. 275–311, Elsevier, 2022.

[35] K. R. Chaturvedi and T. Sharma, "Carbonated nanofluids for EOR and improved carbon storage," *Nanotechnology for CO2 Utilization in Oilfield Applications*, pp. 71–84, 1 2022.

[36] F. Deng, X. B. Luo, L. Ding, and S. L. Luo, "Application of Nanomaterials and Nanotechnology in the Reutilization of Metal Ion From Wastewater," *Nanomaterials for the Removal of Pollutants and Resource Reutilization*, pp. 149–178, 1 2019.

[37] R. J. Baxter and P. Hu, "Insight into why the Langmuir-Hinshelwood mechanism is generally preferred," *Journal of Chemical Physics*, vol. 116, pp. 4379–4381, 3 2002.

[38] Z. Qiao, D. Johnson, and A. Djire, "Challenges and opportunities for nitrogen reduction to ammonia on transitional metal nitrides via Mars-van Krevelen mechanism," *Cell Reports Physical Science*, vol. 2, p. 100438, 5 2021.

[39] B. Hammer and J. K. Nørskov, "Theoretical surface science and catalysis—calculations and concepts," *Advances in Catalysis*, vol. 45, no. C, pp. 71–129, 2000.

[40] L. Liu and A. Corma, "Metal Catalysts for Heterogeneous Catalysis: From Single Atoms to Nanoclusters and Nanoparticles," *Chemical Reviews*, vol. 118, pp. 4981–5079, 5 2018.

[41] C. Isabel Garcia Yago, *Thiolate protected gold catalysts for oxidation reactions*. PhD thesis, TU Wien, Vienna, 2020.

[42] J. Yan, B. K. Teo, and N. Zheng, "Surface Chemistry of Atomically Precise Coinage-Metal Nanoclusters: From Structural Control to Surface Reactivity and Catalysis," *Accounts of Chemical Research*, vol. 51, pp. 3084–3093, 12 2018.

[43] V. Sudheeshkumar, K. O. Sulaiman, and R. W. Scott, "Activation of atom-precise clusters for catalysis," *Nanoscale Advances*, vol. 2, pp. 55–69, 1 2020.

[44] M. S. Bootharaju, C. P. Joshi, M. R. Parida, O. F. Mohammed, and O. M. Bakr, "Templated Atom-Precise Galvanic Synthesis and Structure Elucidation of a [Ag24Au(SR)18] Nanocluster," *Angewandte Chemie International Edition*, vol. 55, pp. 922–926, 1 2016.

[45] B. Panthi, A. Mukhopadhyay, L. Tibbitts, J. Saavedra, C. J. Pursell, R. M. Rioux, and B. D. Chandler, "Using Thiol Adsorption on Supported Au Nanoparticle Catalysts to Evaluate Au Dispersion and the Number of Active Sites for Benzyl Alcohol Oxidation," *ACS Catalysis*, vol. 5, pp. 2232–2241, 4 2015.

[46] T. Mitsudome, M. Yamamoto, Z. Maeno, T. Mizugaki, K. Jitsukawa, and K. Kaneda, "One-step Synthesis of Core-Gold/Shell-Ceria Nanomaterial and Its Catalysis for Highly Selective Semihydrogenation of Alkynes," *Journal of the American Chemical Society*, vol. 137, pp. 13452–13455, 10 2015.

[47] Z. Wu, D. E. Jiang, A. K. Mann, D. R. Mullins, Z. A. Qiao, L. F. Allard, C. Zeng, R. Jin, and S. H. Overbury, "Thiolate ligands as a double-edged sword for CO oxidation on CeO 2 supported Au25(SCH2CH2Ph) 18 nanoclusters," *Journal of the American Chemical Society*, vol. 136, pp. 6111–6122, 4 2014.

[48] X. Nie, H. Qian, Q. Ge, H. Xu, and R. Jin, "CO oxidation catalyzed by oxide-supported Au 25(SR) 18 nanoclusters and identification of perimeter sites as active centers," *ACS Nano*, vol. 6, pp. 6014–6022, 7 2012.

[49] M. Zhu, C. M. Aikens, F. J. Hollander, G. C. Schatz, and R. Jin, "Correlating the crystal structure of A thiol-protected Au25 cluster and optical properties," *Journal of the American Chemical Society*, vol. 130, pp. 5883–5885, 5 2008.

[50] W. Fei, S. Antonello, T. Dainese, A. Dolmella, M. Lahtinen, K. Rissanen, A. Venzo, and F. Maran, "Metal Doping of Au25(SR)18- Clusters: Insights and Hindsights," *Journal of the American Chemical Society*, vol. 141, pp. 16033–16045, 10 2019.

[51] A. Ghosh, O. F. Mohammed, and O. M. Bakr, "Atomic-Level Doping of Metal Clusters," *Accounts of Chemical Research*, vol. 51, pp. 3094–3103, 12 2018.

[52] C. García, S. Pollitt, M. van der Linden, V. Truttmann, C. Rameshan, R. Rameshan, E. Pittenauer, G. Allmaier, P. Kregsamer, M. Stöger-Pollach, N. Barrabés, and G. Rupprechter, "Support effect on the reactivity and stability of Au25(SR)18 and Au144(SR)60 nanoclusters in liquid phase cyclohexane oxidation," *Catalysis Today*, vol. 336, pp. 174–185, 10 2019.

[53] J. A. Rodriguez, S. D. Senanayake, D. Stacchiola, P. Liu, and J. Hrbek, "The activation of gold and the water-gas shift reaction: insights from studies with model catalysts," *Accounts of chemical research*, vol. 47, pp. 773–782, 3 2014.

[54] C. Lavenn, A. Demessence, and A. Tuel, "Au25(SPh-pNH2)17 nanoclusters deposited on SBA-15 as catalysts for aerobic benzyl alcohol oxidation," *Journal of Catalysis*, vol. 322, pp. 130–138, 2 2015.

[55] Y. Li, Y. Chen, S. D. House, S. Zhao, Z. Wahab, J. C. Yang, and R. Jin, "Interface Engineering of Gold Nanoclusters for CO Oxidation Catalysis," *ACS Applied Materials and Interfaces*, vol. 10, pp. 29425–29434, 9 2018.

[56] W. Li, Q. Ge, X. Ma, Y. Chen, M. Zhu, H. Xu, and R. Jin, "Mild activation of CeO2-supported gold nanoclusters and insight into the catalytic behavior in CO oxidation," *Nanoscale*, vol. 8, pp. 2378–2385, 1 2016.

[57] V. Truttmann, H. Drexler, M. Stöger-Pollach, T. Kawawaki, Y. Negishi, N. Barrabés, and G. Rupprechter, "CeO2 Supported Gold Nanocluster Catalysts for CO Oxidation: Surface Evolution Influenced by the Ligand Shell," *ChemCatChem*, vol. 14, 7 2022.

[58] A. Shivhare, S. J. Ambrose, H. Zhang, R. W. Purves, and R. W. Scott, "Stable and recyclable Au25 clusters for the reduction of 4-nitrophenol," *Chemical Communications*, vol. 49, pp. 276–278, 12 2012.

[59] S. Hossain, D. Suzuki, T. Iwasa, R. Kaneko, T. Suzuki, S. Miyajima, Y. Iwamatsu, S. Pollitt, T. Kawawaki, N. Barrabés, G. Rupprechter, and Y. Negishi, "Determining and Controlling Cu-Substitution Sites in Thiolate-Protected Gold-Based 25-Atom Alloy Nanoclusters," *Journal of Physical Chemistry C*, vol. 124, pp. 22304–22313, 10 2020.

[60] A. Sels, N. Barrabés, S. Knoppe, and T. Bürgi, "Isolation of atomically precise mixed ligand shell PdAu24 clusters," *Nanoscale*, vol. 8, pp. 11130–11135, 5 2016.

[61] Y. L. Lee, A. Mnoyan, H. S. Na, S. Y. Ahn, K. J. Kim, J. O. Shim, K. Lee, and H. S. Roh, "Comparison of the effects of the catalyst preparation method and CeO2 morphology on the catalytic activity of Pt/CeO2 catalysts for the water-gas shift reaction," *Catalysis Science & Technology*, vol. 10, pp. 6299–6308, 9 2020.

[62] F. Meunier, "Relevance of IR Spectroscopy of Adsorbed CO for the Characterization of Heterogeneous Catalysts Containing Isolated Atoms Relevance of IR spectroscopy of adsorbed CO for," *Isolated Atoms. Journal of Physical Chemistry C*, vol. 2021, no. 40, 2016.

[63] T. Elgayyar, R. Atwi, A. Tuel, and F. C. Meunier, "Contributions and limitations of IR spectroscopy of CO adsorption to the characterization of bimetallic and nanoalloy catalysts," *Catalysis Today*, vol. 373, pp. 59–68, 8 2021.

[64] X. Liao, Y. Liu, W. Chu, S. Sall, C. Petit, V. Pitchon, and V. Caps, "Promoting effect of AuCu alloying on Au-Cu/CeO2-catalyzed CO oxidation: A combined kinetic and in situ DRIFTS study," *Journal of Catalysis*, vol. 382, pp. 329–338, 2 2020.